

INTER-AMERICAN TROPICAL TUNA COMMISSION
COMISION INTERAMERICANA DEL ATUN TROPICAL

Special Report 10

**ESTIMATING THE UNDERWATER SHAPE OF TUNA LONGLINES
WITH MICRO-BATHYTHERMOGRAPHS**

by

Keisuke Mizuno, Makoto Okazaki, Hideki Nakano, and Hiroshi Okamura

La Jolla, California
1999

TABLE OF CONTENTS

	Page
ABSTRACT.....	1
INTRODUCTION	1
BUILDING A MODEL	2
FIELD EXPERIMENTS.....	5
Experiment 1	6
Experiment 2	7
Experiment 3	8
DISCUSSION	9
Longline shape and current structure	9
Periodic vertical motion of the main line.....	9
Problems with the calculations	10
Estimation of the swimming depth of tunas	11
Practical usage of micro-BTs for estimating longline shape	11
SUMMARY	12
ACKNOWLEDGMENTS	12
REFERENCES	13
FIGURES	15
TABLES	32
APPENDICES	33

ESTIMATING THE UNDERWATER SHAPE OF TUNA LONGLINES WITH MICRO-BATHYTHERMOGRAPHS

by

Keisuke Mizuno*, Makoto Okazaki*, Hideki Nakano*, and Hiroshi Okamura*

ABSTRACT

An estimation method for the three-dimensional underwater shape of tuna longlines is developed, using measurements of depth obtained from micro-bathymographs (BTs) attached to the main line at equally spaced intervals. The shape of the main line is approximated by a model which consists of a chain of unit length lines (folding-rule model), where the junction points are placed at the observed depths. Among the infinite number of possible shapes, the most likely shape is considered to be the smoothest one that can be obtained with a numerical optimization algorithm. To validate the method, a series of experimental longline operations were conducted in the equatorial region of the eastern Pacific Ocean, using 13 or 14 micro-BTs per basket of main line. Concurrent observations of oceanographic conditions (currents and temperature structure) were obtained. The shape of the main line can be calculated at arbitrary times during operations. Shapes were consistent with the current structure. On the equator, the line was elevated significantly by the Equatorial Undercurrent. It is shown that the shape of main line depends primarily upon the vertical shear and direction of the current relative to the gear. Time sequences of calculated shapes reveals that observed periodic (1-2 hours) oscillations in depth of the gear was caused by swinging movements of the main line. The shortening rate of the main line is an important parameter for formulating the shape of the longline, and its precise measurement is desirable.

INTRODUCTION

Tuna longline fisheries operate around the world. For successful operation, hooks should be set at the swimming depths of targeted fish. Fishermen try to control the hook depth mainly by adjusting the degree of sagging of the main line, which can be accomplished while setting the gear by varying the ship speed, the placement of floats, and the speed at which the main line is released. The degree of sagging is defined by the ratio of the horizontal distance between a pair of neighboring floats and the total length of main line between them, and it is referred to as the shortening rate. In operations, the expected shortening rate is estimated using the simple assumption that the mainline makes a catenary on a vertical plane. In reality, the longline is elevated by ocean currents, and eventually the actual hook depths are shallower than those assumed. Hanamoto (1987) reviewed several previous studies based on measured depths, and concluded that the actual depth is generally 10 to 20% shallower than that assumed using the catenary model.

Occasionally the main line is elevated in an unfavorable direction and branch lines become entangled, which prevents efficient operation. Elevation of the main line probably causes movements of hooks and bait at the end of the branch lines. Since underwater movement

*National Research Institute of Far Seas Fisheries, 5-7-5 Orido, Shimizu, 424 Japan

of hooks is hypothesized to have an attracting effect on fish (Tauchi 1963), such movement may enhance catches. Thus, it is desirable to develop a model which would reveal the three-dimensional underwater shape and the movement of longlines under various oceanographic conditions.

Estimation of the shape of longlines is an old problem, attracting the interest of many fisheries researchers. Generally, there are two ways to approach this problem. One is to use a dynamic model in which currents are given and the corresponding shape is solved under the balance of forces. The other is to estimate the shape by using detailed observations of mainline depth data from multiple observations under various conditions. Using the first approach, Shibata (1962) investigated the cases in which current direction was parallel to or was at a right angle to the line, and Morita (1969) investigated the shape using hydraulic tank experiments. These methods are valid only for very simple cases and are not generally applicable. Using the latter approach, Hamuro and Ishii (1958) attached a few depth recorders to longlines and estimated the shape with an analogue scale model, which is a rather subjective method, as we will show. Additionally, attempts to determine the shape with acoustic methods have met with limited success (Kawaguchi *et al.* 1962).

Recently, Mizuno *et al.* (1996) developed a micro-BT system for longliners. It is much smaller than previous systems and is designed for concurrent multi-probe use. By attaching many probes to the main line at equal intervals, the time-depth records that are obtained provide information on the underwater shape of the main line.

In this paper we develop a method to estimate the three-dimensional underwater shape of a longline with observed time-depth data. First, we review the problem and introduce a model which approximates the shape of the line with a chain of unit length. The problem is then treated mathematically as one of searching for optimal solutions. Field testing was performed in tropical waters of the eastern Pacific Ocean with longlines set from a Japanese research vessel. The estimated underwater shape of the longline obtained from the model is then compared with observations obtained from micro-BTs and measurements of oceanographic conditions to validate the method.

BUILDING A MODEL

The underwater shape of a settled main line is a catenary curve on a vertical plane when there is no water motion relative to the gear (Yoshiwara 1954). In reality, there is motion relative to a settled main line, and the shape of the main line is modified so that it takes on a three-dimensional shape. If the depth of the main line is observed at an adequate number of equally spaced points within a basket (*i.e.* within a portion of the main line between a pair of neighboring floats), Z coordinates of these points are obtained. In this case, given the horizontal distance between the floats, horizontal coordinates (X and Y) can also be estimated. Thus, the three-dimensional shape of the main line can be estimated.

Hamuro and Ishii (1958) tried to simulate the shape of a main line with a scale model (Figure 1). They observed the depth of a main line at three positions with a mechanical depth meter. The observed depths were then simulated on the scale model by adjusting the height of three metal rods. The displacement of each rod from the "natural" shape of the thread (main

line) was noted. Since they did not define the term “natural”, the method was subjective, but, in spite of this, their approach hits at the point of this problem. If we replace the word “natural” with smoothest, the problem is to find the smoothest curve which penetrates given Z coordinates of the points.

Hydrographic features that create shear, such as eddies, inertial currents, and internal waves, can create line shapes which would be judged radical. However, such radical shapes indicate that internal tension in the main line has been temporarily overcome by external forces, and such a state can not continue for a long time. Inspecting previously reported records from depth meters attached to longlines (*e.g.* Hamuro and Ishii, 1958, Fujii and Okamoto 1969, Nishi 1990, Mizuno *et al.* 1996), depth changes occur slowly and the longline is generally quite stable. Such being the case, it might be reasonable to assume that the shape of the line between two floats is generally smooth. This assumption seems to be the general sense of the physical meaning of “natural” in Hamuro and Ishii (1958).

The problem can be defined as follows:

- 1) There is a flexible line in a three-dimensional space, and its total length is known.
- 2) The ends of the line are on a horizontal plane, and distance between them is known.
- 3) The Z -coordinates of N equally spaced points along the line are known.

In order to determine the shape of the main line, coordinates of all points of the line are determined. Continuous function(s) are needed to express the coordinates. For simplicity, a linear function was selected for use herein. The curve was approximated by a chain of unit-length lines connected at junctions like a folding rule (hereafter referred to as the folding-rule model). The shape of the line may then be expressed by a set of coordinates of $N + 1$ junction points as follows:

$$P_i = (X_i, Y_i, Z_i) \quad (i = 0, 1, 2, \dots, N) \quad (1)$$

The case with $N = 4$ is shown in Figure 2. One end of the line, P_0 , is placed on the origin, and the other end, P_N , is placed on the X axis. Since line segments are of unit length (=1), total line length is N . Designating the horizontal distance between P_0 and P_N as L , it can be expressed as

$$L = KN \quad (2)$$

where K is the shortening rate. The coordinates of the ends of the line are given by:

$$P_0 = (0, 0, 0), \text{ and } P_N = (KN, 0, 0)$$

where K is the shortening rate, which is given. Z_i are obtained by observation. The folding-rule model can now be treated as a set of unit vectors:

$$\vec{V}_i \quad (i = 0,1,2,\dots,N),$$

and each vector may be expressed in polar coordinates as shown in Figure 2, such that:

$$\vec{V}_i = \vec{P}_i - \vec{P}_{i-1} = (\cos\phi_i \cos\theta_i, \cos\phi_i \sin\theta_i, \sin\phi_i) \quad (i = 0,1,2,\dots,N) \quad (3)$$

where ϕ_i and θ_i are, respectively, latitudinal, and longitudinal angles of the vector, with respective ranges $-90^\circ < \phi_i < 90^\circ$ and $-180^\circ < \theta_i < 180^\circ$. Since the depth Z_i is given by observation, ϕ_i is determined. Then $\sin\phi_i$ and $\cos\phi_i$ are expressed by d_i and r_i , respectively, and equation (3) may be written as:

$$\vec{V}_i = (r_i \cos\theta_i, r_i \sin\theta_i, d_i) \quad (4)$$

Thus, the line shape can be expressed by N of θ_i . Now the problem becomes one of finding a set of θ_i which makes the shape smoothest, under the conditions that the end points (P_0, P_N) are located at origin and at $(KN, 0, 0)$, respectively. Details on the method used to estimate the set θ_i are described in Appendix A.

Since the folding-rule model is an approximation of a smooth curve by a chain of straight lines, it is necessary to consider the error this may introduce into the model. It is expected that the error would decrease with increasing numbers of segments. However, increasing the number of segments increases the required calculations, as well as the required number of micro-BTs. Thus, the optimum number of segments should be that judged sufficient (*i.e.* providing tolerable error), but also cost effective.

The difference between a given shape and the fitted folding-rule model should be evaluated quantitatively. However, the fit of the model to a smooth line depends upon the shape of the line, so each shape of interest should be examined. We demonstrate the general approach with an application to the most typical situation, the catenary.

The error involved in approximating a continuous catenary with a two-segment model is shown in Figure 3. Since both midpoints of folding rule (P) and catenary (Q) are placed on the same depth and their segment length are of unit, the folding rule cannot lie on the vertical plane (*i.e.* x-z plane). If we consider a pair of points (*i.e.* PQ in this case), one on the catenary and the other on the fitted model, then the squared distance between them might be considered for use as a measure of error. However, making this calculation for a large number of such points would be quite tedious, so only the junction points and corresponding points on the catenary were used in calculations of error (Appendix B).

Figure 4 shows error, normalized by the length of main line in a basket, for two, four, six, and eight segments and for four shortening rates within the range of those commonly observed. As expected, the normalized error decreases rapidly with increasing numbers of segments. However, using more than six segments does not reduce the error so much for all shortening rates. Consider a basket of main line of length 500 m, which is a length commonly seen in actual

operations. Using a model with six segments results in error rates on the order of 1 percent (*i.e.* 5 m) at all shortening rates. The error level would be acceptable in practical purposes. Also, using six segments is reasonable in view of cost-effectiveness.

FIELD EXPERIMENTS

Taking advantage of a tuna-resources research cruise of the R/V *Shoyo Maru* (1,362 GT, cruise FY96-1), we conducted a series of experiments in the tropical eastern Pacific during July 1996 to validate the folding-rule model. The experiments were conducted three times, at different locations (hereafter, Experiments 1, 2, and 3; Table 1).

In each experiment, a longline with 54 baskets, each with 13 branch lines, was set (Table 2). Fifteen micro-BT probes (Murayama Electric Co. SBT-500, see Mizuno *et al.* 1996) were attached (in the fifth basket of each set) to the top of 13 branch lines and to the bottoms of two float lines (Figure 5). The data sampling interval was 10 seconds. Since a probe is light and small (37g in water, 170 mm long and 18 mm in diameter), its effect on the shape of longline was considered to be negligible. Temperature/depth data from the probes were corrected for measurement error with a comparison test in which all probes were tied to a CTD (SBE 911 plus) and lowered to 500 m. Data correction was based on linear curve fitting. The adjusted depths for the probes have an accuracy of ± 1.5 m at depths of up to 500 m. Locations for the experiments were selected to investigate the response of line shape under different current regimes (Figure 6a). Launching/retrieving positions of floats for every 10 baskets were measured by global positioning satellite (GPS, Figures 6b-d).

During the longline operations, vertical current profiles were measured by acoustic Doppler current profiler (ADCP; 75 kHz), for each 8-m depth bin from 16 m (offset) to about 400 m. Pinging interval was about 1 second, and the data were averaged over an interval of 5 minutes. Also, expendable bathythermographs (XBTs) were dropped at the midpoint of each setting of the longline.

Shortening rate is an important parameter for calculation of the shape. However, it is difficult to continuously measure the horizontal distances between floats. We can observe the distance at launching/retrieving by using the position of the ship. Since the float positions in Figures 6b-d were measured at different times, they don't show actual distance, and adjustment is necessary when estimating shortening rate. Some effort should be made to obtain accurate shortening rates.

Suppose that a float A was launched at time t and position $P(t)$ and was later retrieved at a known time and position (Figure 7). From these data we can obtain the mean drifting velocity, \vec{V} . When the next float on the main line, B, is launched at time $t + \Delta t$ at position $Q(t + \Delta t)$, float A is no longer at $P(t)$, as it has moved from point A by a distance of $\vec{V}\Delta t$. The distance between floats A and B at time $t + \Delta t$ is not the length of the vector $P(t)Q(t + \Delta t)$; rather, it is the length of the vector $P(t)Q(t + \Delta t)$, which is corrected by $\vec{V}\Delta t$. The same method may be applied to positions at retrieval. Shortening rates (Table 3) were estimated from the corrected distances between pairs of floats separated on the main line by 10 baskets, with the experimental basket at the approximate center of the 10 baskets, *i.e.* as basket 5 or 6. Also shown in Table 3

are shortening rates for each experiment. These were derived from the ratio of the velocity of the ship (relative to the water) and the velocity at which the main line was released from the vessel.

Experiment 1

The gear generally drifted eastward, but it rotated counter-clockwise (Figure 6b). Since the sea-surface wind was negligible (Table 1), the rotation may have been due to horizontal velocity shear of the Equatorial Undercurrent (EUC), which is an eastward current that has its maximum velocity at the equator and which has counterclockwise relative vorticity.

Vertical current and temperature profiles are shown in Figure 8. The current profiles were obtained by averaging all data obtained during the launching of the gear, because higher data quality is expected due to stable ship speed and direction. The upper-layer water, from the surface to 50 m, flows northward, and its lower boundary is consistent with the depth of the thermocline. Below the upper layer, eastward flow (*i.e.* the EUC) is dominant between 60 and 160 m, with the maximum velocity at 90 m. Temperature profiles show a 13-14°C layer at 70 to 100 m, which characterizes the EUC (13°C at that depth in equatorial waters; Montgomery and Stroup 1962). Vertical current profiles clearly show a two-layer flow structure, with a northward-flowing surface layer and a strong eastward-flowing undercurrent layer, and with strong vertical shear between.

Time/depth records from micro-BTs are shown in Figure 9. It is noted that the bottom of the float line was quite stable. However, once the main line sank to a maximum depth (at about 8:00), it shoaled and then stayed at shallower depths. When it reached maximum depth, the central branch line (number 7) was not the deepest; rather, number 9 was the deepest. This means that the main line was asymmetrical.

The shape of the main line was calculated every 15 minutes during the operation, using the described method. The shortening rate was assumed to be constant during the operation and equal to the mean value of 0.81 observed at launching and retrieving (Table 3). The shape of the main line at the points of greatest and settled depths, 8:00 and 10:45, respectively, are shown in Figure 10. Drifting velocity and current velocity maxima in the upper and lower layers are shown schematically, along with perspective views of line shape, at 8:00 (upper panel, Figure 10). Relative current velocity can be obtained by subtracting the drifting velocity from the current velocity. Three planar views of line shape and relative current velocity at the middle point of each segment are also shown in Figure 10. The shape at 8:00 was skewed to the right (front view) by the eastward-flowing EUC dragging the deeper parts of the longline obliquely to the south-southeast. In addition, the mid-depth segment of the longline was dragged eastward (side view).

The shape at 10:45 (lower panel, Figure 10) was elevated drastically, which is clearly shown by the side view; however the relative current was quite weak. This suggests that the weak dragging force was balanced by gravity, resulting in a nearly symmetrical shape approximating the catenary form, but which was displaced from the vertical. The front view shows that the center of the main line (*i.e.* the top of branch line 7) reached a depth of no more than 70 m. The central part of the line at 60 to 70m (branch lines 5-9) were located in the EUC, while the shallower parts of the line were located in the northward-flowing current of the upper

layer.

Experiment 2

The gear drifted to the east-southeast at a rate of 0.4 knots (Figure 6c). Since the sea-surface wind was weak, its effect on the drift was assumed to be negligible. Vertical current profiles (Figure 11) show southeastward flow in the upper 200 m, which was consistent with the direction and velocity of drift. The profiles were comparatively uniform with depth, so the vertical shear was much less than that in Experiment 1 for both zonal and meridional components.

The zonal component of velocity was nearly zero from the surface to a depth of 60 m. Below 60 m, it reached a maximum at 90 m, and then gradually decreased with depth. The current at depth had a maximum velocity nearly equal to that of the EUC, although its location was nearly at 5°S. This current was likely to be that identified by Tsuchiya (1975) as the “subsurface countercurrent.” He described it as a pair of narrow bands of current located symmetrically about the equator at about 5° north and south. They are clearly separated from the EUC in the tropical eastern Pacific, with underwater high velocity cores situated slightly deeper than that of EUC. Recently, Watanabe and Mizuno (1993) detailed the current structure of the pair of bands in detail by ADCP (Figure 12). The observed current in this experiment was estimated to be the southerly component of the subsurface countercurrent.

Time/depth data of 14 micro-BTs (one attached to the bottom of the float line failed) are shown in Figure 13. The bottom depth of the float line was constant, as observed in Experiment 1. The main line settled at depth about 20 minutes after launch, and the depths of the branch lines were generally stable during the set. However, a vertical periodic motion with a period of 1 to 2 hours was observed. The maximum depth at each position on the line was reached at 9:15. After settling, the central part of the line (*i.e.* branch line 7) was the deepest, and pairs of branch lines equidistant from the center of the longline were located at similar depths. This means that the shape of the line was approximately symmetrical.

The shape of the longline was calculated for each 15 minute period, as in Experiment 1, but with a constant shortening rate of 0.84. In Figure 14, two typical shapes are shown. One is the shape observed at 9:15, when the longline reached its greatest depth (upper panel), and the other is the shape at 11:30, when the line was at moderate depth.

The drifting velocity and the velocity of the upper and lower layers had similar directions (upper panel), and the currents relative to the line were generally weak in both layers. The deepest part of the line descended to 200 m. The horizontal displacement of the line was generally small. The line shape at 9:15 was not skewed laterally (front view), which is explained by the very weak lateral flow shown in the relative current diagram. The shape was nearly on a vertical plane; however the relative current was not weak (side view). Since the shape varied, this current may have tended to push the line upward.

The shape of the line at 11:30 was also symmetrical, because of the relatively weak lateral flow (front view). The line is elevated slightly (side view), and the relative current flows in the same direction at each segment. Although it is hard to check the balance of force

quantitatively, the current direction was consistent with the shape.

The sequential inspection of the estimates of shape at 15-minute intervals (not shown), a swinging movement of main line was clearly seen, which is consistent with a periodic vertical motion that is in phase with all records shown in Figure 13. This suggests that the current velocity caused perturbations in the depth of the line in this experiment.

Experiment 3

In this experiment the gear was located in the South Equatorial Current (SEC) at 6° 30'S, and generally drifted to the west-southwest. The vertical current profile (Figure 15) shows that the zonal component was westward and strong, about 30 cm/s, from the surface to 70 m, dropping off significantly below this depth. The meridional component was southward and relatively weak throughout the water column. These observations were consistent with the vertical temperature profile, which indicated a surface mixing layer in the upper 70 m of the water column and a thermocline between 70 and 100 m.

Time/depth data from micro-BTs are shown in Figure 16. The depths of the bottoms of the float lines were constant, as in previous experiments. In this experiment the main line appeared to settle within about 15 minutes of launching. However, in contrast to the observations in Experiments 1 and 2, the main line slowly sank, reaching a maximum depth at about 10:30, after which it gradually shoaled. Although the central branch line (*i.e.* number 7) was the deepest during most of the operation, branch lines 8-13 were deeper than their counterparts at the other end of the main line. Thus, the main line was asymmetrical.

Again, the shape of the longline was calculated for each 15-minute period. However, in this case the shortening rate obtained by GPS at launching exceeded 1.0 (Table 3), so the ratio of ship speed (relative to the ocean surface) to the releasing speed of the longline, 0.94, was used. This value was the greatest among the experiments.

Calculated shapes for Experiment 3 are shown in Figure 17 for 7:45, at which time the depth of the line was increasing, and 10:30, at which time the line had reached its maximum depth. The shape at 7:45 was not significantly skewed, because only the end points of the line were exposed to fairly strong currents, while most of the line was exposed to no significant flow (front view panel). However, the line was slightly elevated by relatively weak shear occurring along the direction of drift (side view panel). The shape at 10:30 was skewed slightly to the east-southeast because the deeper parts of the line were subjected to currents flowing in that direction (front view panel). By 10:30 the line was hanging vertically in the water column, even though it was in a field of relatively weak currents (side view panel).

The main difference between the shapes observed at 7:45 and 10:30 is the maximum depth of the line. At 7:45 (upper panel) the line was generally shallower and hanging slightly off the vertical, as compared to the shape at 10:30. This occurred because the line was set with a large shortening rate. Close inspection of the shape at 10:30 shows that the east-southeast end point of the main line was shifted slightly toward the west-northwest. Such a shift means that the solutions obtained (a set of θ_i) did not satisfy the observations and underlying assumptions of the model: specifically, given the estimated shortening rate (0.94) and observed depths of the

line, the model predicted a shorter span between the endpoints of the line than was observed.

The actual shortening rate for this experiment was likely to have been less than that estimated by the ratio of vessel velocity and releasing speed of the line (*i.e.* 0.94). The shortening rates estimated by GPS during this experiment decreased from 1.01 at the start of the operation to 0.86 as the operation continued. This implies that as the line was set the portions placed in the water early in the process initially would have been shallower than those portions placed later. Then, as time passed, the line gradually settled, so that the “true” shortening rate observed once the line had settled (*i.e.* by 10:30) was less than that estimated on setting of the gear.

DISCUSSION

Longline shape and current structure

The calculated shapes clearly reveal the degree of rising toward the surface and asymmetry of the line. The shapes were consistent with the vertical current shear relative to the line as estimated by ADCP data and the drifting velocities of the longline. The drifting velocity depends on currents from the surface to the bottom of the line.

In Experiment 1 the degree of rising to the surface of the line was large. In this case, the vertical current shear was strong between the surface SEC and subsurface EUC. On the other hand, in Experiment 2 there was only weak current shear, though the current itself was relatively strong, and the observed line shape was a nearly vertical catenary. Vertical current shear in the SEC made the line asymmetric in Experiment 3. In all three cases, the line shape was consistent with the observed vertical current shear.

If the sea surface wind is negligible and there exists vertically-uniform flow, then the line would not experience differential flow rates across its length, and its parts would move at a uniform speed along with the surrounding water. In this case, the external forces working on the line are gravity and buoyancy, and the line shape resulting from a balance of these is a catenary on a vertical plane. In the presence of differential vertical current shear across the length of the main line, dragging and lifting forces will modify the shape and motion of the line.

Periodic vertical motion of the main line

The sea state during the experiments was generally quiet, without large, long-period swells and large surface waves, which might be evident in micro-BT data averaged over short periods (10s of seconds). The bottoms of the float lines remained at constant depths during the experiments, which means that both ends of the lines in a basket were vertically fixed. However, other parts of the line showed quasi-periodic vertical movements. Such movements have been detected previously using a few depthmeters attached to mainline (*e.g.* Fujii and Okamoto 1969, Nishi 1990), but overall view of mainline movements have not demonstrated. In our experiments, all parts of the line moved in phase, with movement of the deeper parts showing greater amplitudes. By inspecting the successive 15-minute calculations of line shape (not shown), the pendulum-like, back-and-forth swinging motion of a line hanging from fixed endpoints was clearly shown. The swinging motion appeared in all three experiments, but its amplitude and period varied in each experiment. A basket of mainline hanging from fixed points

in stationary water should swing with a certain period like a pendulum. In reality, vertical current shear is added as an external force to this system. If vertical current shear changes periodically, the mainline would make a forced swinging motion. Even constant vertical shear would cause the mainline self-induced swinging motion. In any case, observed swinging motion is caused by vertical current shear, and the nature of the motion will be investigated by numerical simulation model in the future.

Problems with the calculations

It was shown that an accurate estimate of the shortening rate is necessary for calculation of the shape of the main line. One of the error sources of the shortening rate is measurement error of horizontal distance between a pair of floats. The distance was estimated using GPS positions of a pair of floats (actually positions of ship at launching and retrieving of floats). In one instance the calculated rate from GPS data exceeded 1, which was probably due to the limited accuracy of the GPS system. It would be desirable to reduce the error rate by one order of magnitude (*i.e.* to 1 percent), which would be equivalent to estimating distance between floats to within several meters along a typical main line with a length of several hundred meters.

Also the distance should be measured continuously, because the distance possibly changes during the gear is drifting. In Experiment 3, the shortening rate changed by 15 percent, which suggests that shortening rates may change by about 10 percent during normal operations. Such continuous and accurate measurement might be available using GPS buoys. For distance measurement, relative locations of the floats are needed but not absolute locations. Simultaneous positioning by GPS buoys might give more accurate relative locations of them than repeated positioning using single GPS system, which is the same idea as DGPS (differential GPS). It is recommended that GPS buoys be used whenever possible in future experiments.

Another error source of the shortening rate is change of mainline length itself. Although we are able to measure it accurately on board, there is a possibility that lengthening of the main line, caused by tension on the line when deployed, could introduce an error into the estimate of shortening rates. To check the significance of that possibility, we measured the expansion rate. It was calculated to be about 1.5 percent for a 10-kg weight. To examine the impact of tension on a main line *in situ*, a line in the shape of a vertical catenary and with a shortening rate of 0.94 (as assumed in Experiment 3) was used. A 7.8 kg-weight was placed on the line and the expansion rate determined. In this instance the rate was less than 1 percent. We therefore consider that tension did not introduce significant change of the mainline length or the shortening rate.

If an assumed shortening rate is greater than the actual rate, this model will produce an estimate of a shape closer to the vertical plane than actual one. Although greater shortening rate tends to make the line shallower in general, the model uses the observed depth of the line. Therefore, the model obliged to make the line smaller in horizontal distance from the vertical plane. In a drastic case when the observed depths exceed the limits of depth caused by overestimating shortening rate, no real-valued, non-zero set of θ_i will provide a solution to equation A.3 (Appendix A). This was the case in Experiment 3. Although the main line was actually deployed tightly (*i.e.* with a large shortening rate) at the beginning, it seems to have been considerably loosened (*i.e.* achieving a lesser shortening rate) over time. Since the rate is a

constant in the model, the rate estimated early in the set was an overestimate of the shortening rate when the line later reached its maximum depth.

Estimation of the swimming depth of tunas

Knowledge of the swimming depth of tunas is important to effective fishing and to understanding estimates of catch rates which may be influenced by the distribution of fish and fishing gear within the water column. Previous studies of swimming depth (*e.g.* Suzuki *et al.* 1977) and standardized catch rates (*e.g.* Hinton and Nakano 1996) have estimated the depth of capture of fish on individual branch lines by assuming that the shape of the main line was a catenary in a vertical plane. Such methods may be improved upon by incorporating information on ocean currents in estimates of the shape.

Our model is capable to estimate line shape from observed depth data as model input, but not capable to predict line shape (i.e. a set of θ_i 's) from current data as model input.

However, results of experiments confirmed that the shape of the line depends on current shear relative to the main line. It encourages us future development of a dynamic model which outputs line shape from input of current data. On the other hand, continuation of *in situ* experiments will supply empirical estimation of line shape from current data.

The time scale of a longline operation is about 12 to 20 hours, so the optimal estimation of the shape must be based on the concurrent current structure, which is available only from vessels equipped with ADCPs. In addition, collection of oceanographic data from buoy arrays may provide appropriate data for use in estimating line shapes in various regions. For example, a recently-deployed buoy array in the equatorial Pacific (McPhaden 1995) may supply nearly real-time information in a limited area. However, in a first approach to use of this model, large-scale geostrophic current shear derived from mean density fields may prove valuable, with shear calculated from climatological data (*e.g.* Levitus *et al.* 1994, Levitus and Boyer 1994).

In a few operations during the cruise, micro-BT data detected fish-hooking, which revealed the hooking-time/depth/temperature and vertical location of the fish. Such data are extremely valuable, and an adequate amount of data for obtaining statistically-significant estimates of swimming depth might be obtainable. Nakano and Bayliff (1992) estimated that hooking rates for tunas and tuna-like species is generally about 1 percent. Assuming the 1 percent rate, 10,000 micro-BT observations are necessary to obtain 100 observations of fish-hooking on branch lines with micro-BTs. In order to attain this sampling level, we would need 10 longliners, each with half dozen micro-BTs, and each making 150 to 200 sets a year. While this may be somewhat difficult, it still seems to be a feasible level of sampling.

Practical usage of micro-BTs for estimating longline shape

Considering the simplicity of model calculation, it is easier to deploy micro-BTs at equally-spaced interval. For the safety and reliability of the task of in-situ experiment, it is preferable to attach micro-BTs to the mainline at the same positions of branch and float lines.

Previously, it is shown that 6 segments are necessary and sufficient for estimating longline shape for practical purposes, which requires 7 micro-BTs. In the operations using 5 to

10 branch lines a basket, it is recommended to attach the BTs to the main line at every positions of float and branch lines for the simplicity of the task. When using more than 11 branch lines a basket, we are able to save micro-BTs attaching them at the positions of every other branch lines (in the case of odd number of branch lines). It is more valuable to deploy saved micro-BTs on other baskets rather than deploying all of them on one basket. It provides us doubled information of line shapes.

SUMMARY

We propose a method to estimate the three-dimensional underwater shape of a longline, using time/depth records from micro-BTs which are attached to the main line at equally-spaced intervals. In order to validate this method, field experiments were conducted in the tropical eastern Pacific Ocean at three locations in three different current regimes. The estimated shape of the longline and its movements were compared to the observed hydrographic conditions, and the validity of this method was examined. We obtained the following major results:

1) The underwater shape of a basket of gear on the main line may be approximated by a folding-rule model, which consists of a chain of unit-length line with flexible junctions at specified points along the line. For the calculations, only Z coordinates of the points and the horizontal distance between the ends of the line were observed. The X and Y coordinates of each point were calculated under conditions which make the shape the smoothest (*i.e.* which minimize the squared sum of curvature at the points). Solutions were obtained with the multiplier method for numerical nonlinear optimization problems.

2) A model having six or more segments is adequate to describe the shape of line accurately.

3) The bottom end of the float line remained at a nearly constant depth during the operations, which suggests that end points of the baskets along the main line were strongly restricted in terms of vertical movement.

4) Calculated line shapes depended on the vertical current shear relative to the line, rather than on current speed. Also, shear was found to cause a swinging-like movement of the line from the vertical plane and/or an asymmetric shape. A set of time/depth records in a basket showed quasi-periodic synchronized vertical motion that was caused by the swinging movement of entire line of the basket, which was consistent with and supports the validity of the method.

5) In order to obtain a correct estimate of line shape, an accurate and continuous estimate of the shortening rate is necessary. As part of future research, it would be desirable to measure continuously the distance between a pair of neighboring buoys using a GPS system installed on floats.

ACKNOWLEDGMENTS

We extend our appreciation to Dr. Kazuhiko Hiramatsu and Mr. Yukio Takeuchi of the National Research Institute of Far Seas Fisheries for their helpful discussions on the calculation method. The experiments at sea were made possible by the significant and united efforts of Captain Kan'ich Yamanaka of R/V *Shoyo Maru* and his crew. Our thanks are extended to Dr.

Michael G. Hinton of the IATTC, who kindly checked the first draft of this paper and gave us helpful comments. We also thank Dr. William H. Bayliff and Dr. George Watters of the IATTC for reviewing the manuscript.

REFERENCES

- Fujii, I., and H. Okamoto. 1969. On the shape of tuna longline gear under water and catches of tunas and billfishes. Tech. Rep. Mie. Pref. Hamajima Fish. Exp. Sta.: 45-103 (in Japanese).
- Hamuro, T., and K. Ishii. 1958. Analysis of tuna long-line by automatic depth-meter. Tech. Rep. Fish. Boat., **11**: 39-119 (in Japanese with English abstract).
- Hanamoto, E. 1974. Fishery oceanography of bigeye tuna - I. Depth of capture by tuna longline gear in the eastern tropical Pacific Ocean. La Mer, **12** (3): 128-136 (in Japanese with English abstract).
- Hanamoto, E. 1987. Effect of oceanographic environment on bigeye tuna distribution. Bull. Japan. Soc. Fish. Oceanogr., **51** (3): 203-216.
- Hinton, M. G., and H. Nakano. 1996. Standardizing catch and effort statistics using physiological, ecological, or behavioral constraints and environmental data, with an application to blue marlin (*Makaira nigricans*) catch and effort data from Japanese longline fisheries in the Pacific. Bull. Inter-Amer. Trop. Tuna Comm., **21** (4): 165-200.
- Kawaguchi, K., M. Hirano, and M. Nishimura. 1962. Detection of underwater shape of tuna longline by fish finder. Tuna Fisheries: 91-109 (in Japanese).
- Levitus, S., R. Burgett, and T. P. Boyer. 1994. World Ocean Atlas 1994, Volume 3: Salinity. NOAA Atlas NESDIS 3: 111 pp.
- Levitus, S., and T. P. Boyer. 1994. World Ocean Atlas 1994, Volume 4 : Temperature. NOAA Atlas NESDIS: 129 pp.
- McPhaden, M. J. 1995. The Tropical Atmosphere and Ocean array is completed. Bull. Amer. Meteorol. Soc., **76** (5): 739-741.
- Mizuno, K., M. Okazaki, H. Nakano, and H. Okamura. 1997. Estimation of underwater shape of tuna longline by using micro-BTs. Bull. Nat. Res. Inst. Far Seas Fish., **34**: 1-23 (in Japanese).
- Mizuno, K., M. Okazaki, T. Watanabe, and S. Yanagi. 1996. A micro bathythermograph system for longline boats in view of large scale ocean observing system. Bull. Nat. Res. Inst. Far Seas Fish., **33**: 1-15.
- Montgomery, R. B., and E. D. Stroup. 1962. Equatorial waters and currents at 150°W in July-August 1952. Johns Hopkins Oceanographic Studies, **1**: 68 pp.

- Morita, T. 1969. Studies on the fishing gear of tuna long-line. Mem. Fac. Fish. Kagoshima Univ., **18**: 145-215 (in Japanese with English abstract).
- Nakano, H., and W. H. Bayliff. 1992. A review of the Japanese longline fishery for tunas and billfishes in the eastern Pacific Ocean, 1981-1987. Inter-Amer. Trop. Tuna Comm., Bull., **20** (5): 183-355.
- Nishi, T. 1990. The hourly variations of the depth of hooks and the hooking depth of yellowfin tuna (*Thunnus albacares*), and bigeye tuna (*Thunnus obesus*), of tuna longline in the eastern region of the Indian Ocean. Mem. Fac. Fish. Kagoshima Univ., **39**: 81-98 (in Japanese with English abstract).
- Ohno, Y., and K. Isoda (editors). 1990. Numerical Calculation Handbook. Ohm-sha, Tokyo: 1153 pp (in Japanese).
- Shibata, K. 1962. Analysis of the fish finder records - I. Some information on underwater formation of tuna long-line. Bull. Fac. Fish. Nagasaki Univ, **13**: 9-17 (in Japanese with English abstract).
- Suzuki, Z., Y. Warashina, and M. Kishida. 1977. The comparison of catches by regular and deep tuna longline gears in the western and central equatorial Pacific. Bull. Far Seas Fish. Res. Lab., **15**: 51-89.
- Sverdrup, H. U., M. W. Johnson, and R. H. Fleming. 1942. The Oceans: their Physics, Chemistry, and General Biology. Prentice-Hall, Englewood Cliffs, N.J.: 1087 pp.
- Tauchi, M. 1963. Fisheries Physics. Koseisya-Koseikaku, Tokyo: 116 pp (in Japanese).
- Tsuchiya, M. 1975. Subsurface countercurrents in the eastern equatorial Pacific Ocean. Jour. Mar. Res., **33** (Supplement): 145-175.
- Watanabe, T., and K. Mizuno. 1993. Equatorial current system observed by ADCP in the matured phase of El Niño 1991-1992. Scientific Cruise Report of R/V *Kaiyo Maru* (1st cruise in FY 1991), Fisheries Agency, 246 pp (in Japanese with English abstract).
- Yoshihara, T. 1954. Distribution of catches of tuna longline-IV. On the relation between κ and φ_0 with a table and a diagram. Bull. Japan. Soc. Sci. Fish., **19** (10): 1012-1014.

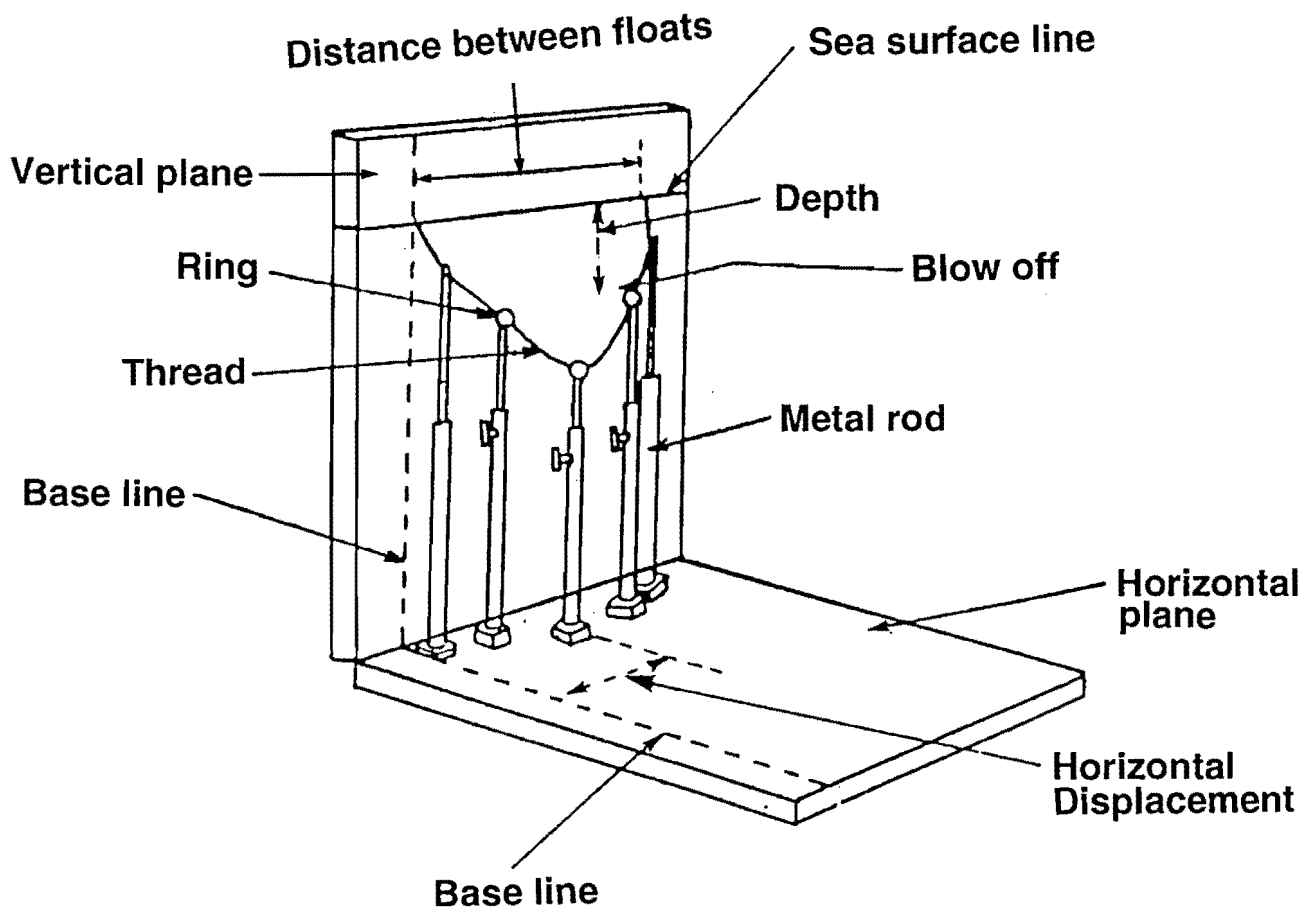


FIGURE 1. A simulator of longline shape by Hamuro and Ishii (1958). The shape is reproduced by using silk thread in a 1/1000 scale model. Rod heights are adjusted with data from depth recorders that were attached to a main line.

$$N = 4$$

$$|\vec{V}_i| = 1 \quad (i = 1, 2, \dots, N)$$

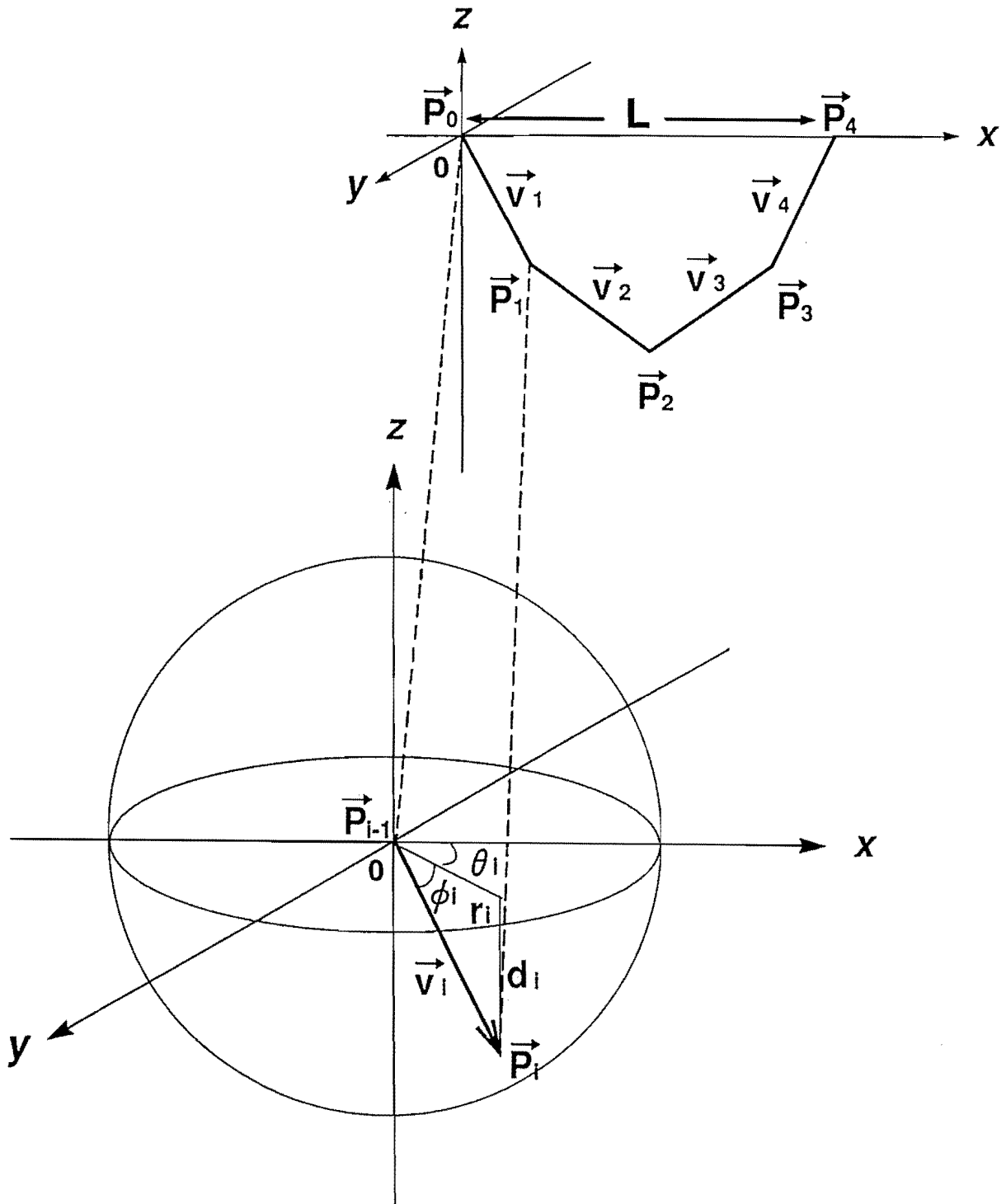


FIGURE 2. Upper panel: A folding-rule model to simulate line shapes. The model having four line segments (unit vector V_1 through V_4) is displayed. Position vectors P_0 through P_4 denote the location of junction points. The distance L between P_0 and P_4 is proportional to the shortening rate, and is determined by observation. Lower panel: Detailed explanation of V_i . The vector V_i may be expressed by latitude (ϕ_i) and longitude (θ_i) in a polar coordinate system. The latitude is obtained from the observed depth, d_i . The longitude (θ_i) is estimated by numerical methods.

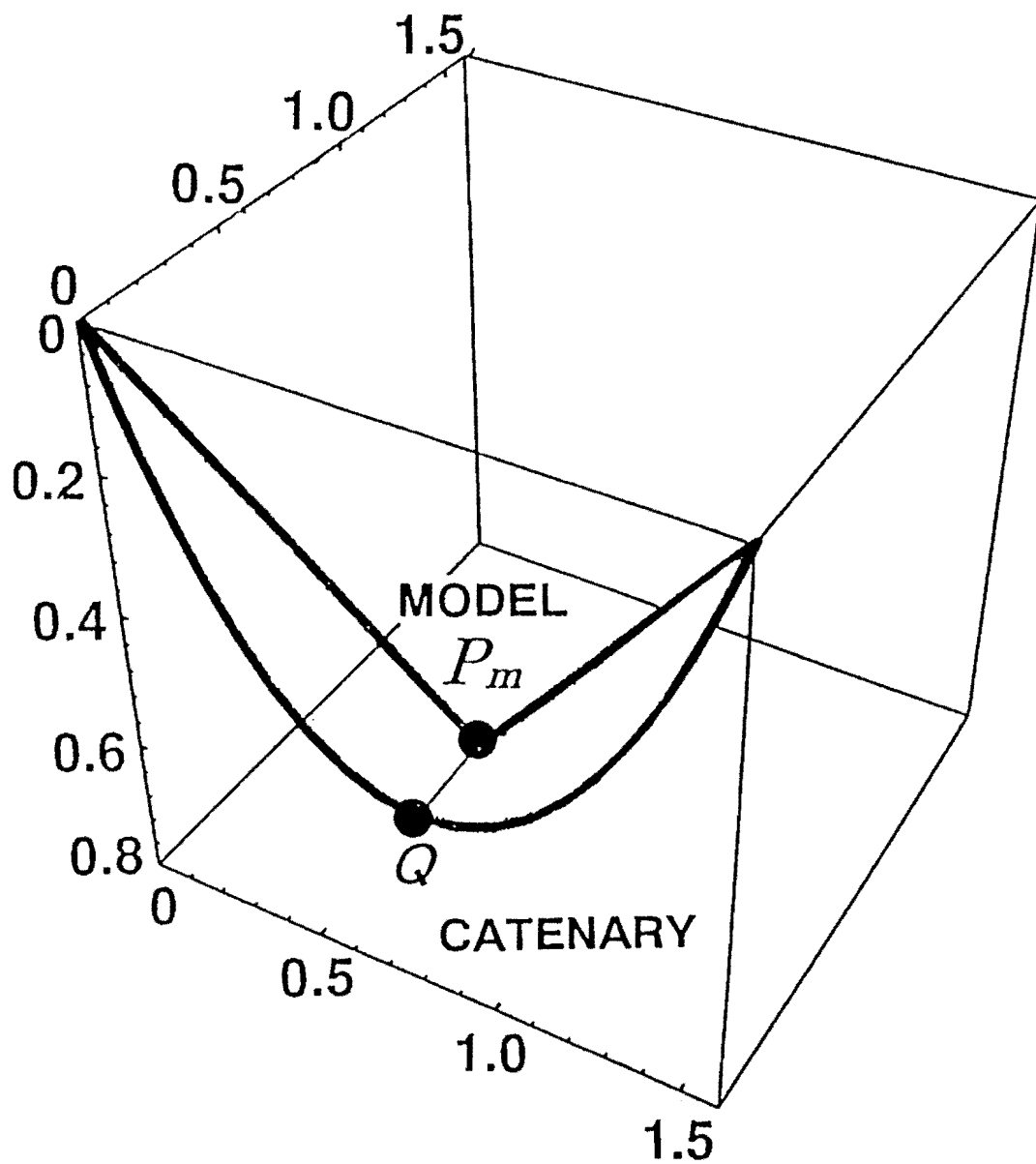


FIGURE 3. Differences between the catenary and the fitted folding-rule model. The model shown has two line segments for simplicity. The junction point of the model has the same depth as the observed depth of the middle point of the catenary. The pair of points P and Q are located equidistant from the origin along the respective lines. The average length of the line PQ provides a measure of the error of the fitted model.

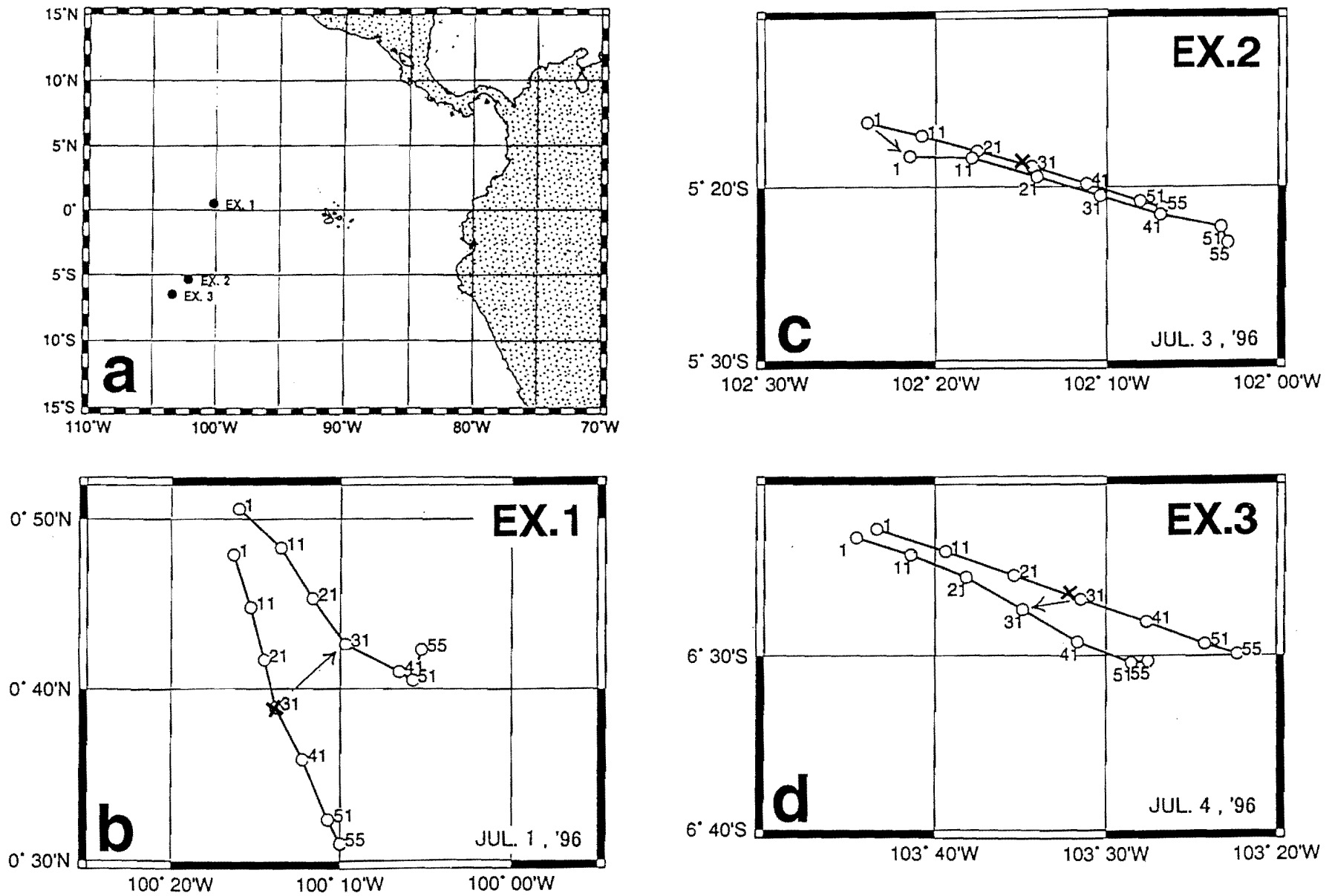


FIGURE 6. Experimental area and longline drift.

Panel a: Locations of Experiments 1-3.

Panels b, c, and d: Launching and retrieval positions for every tenth float (open circles). The directions of drift are given by arrows, and X marks positions of XBT drops.

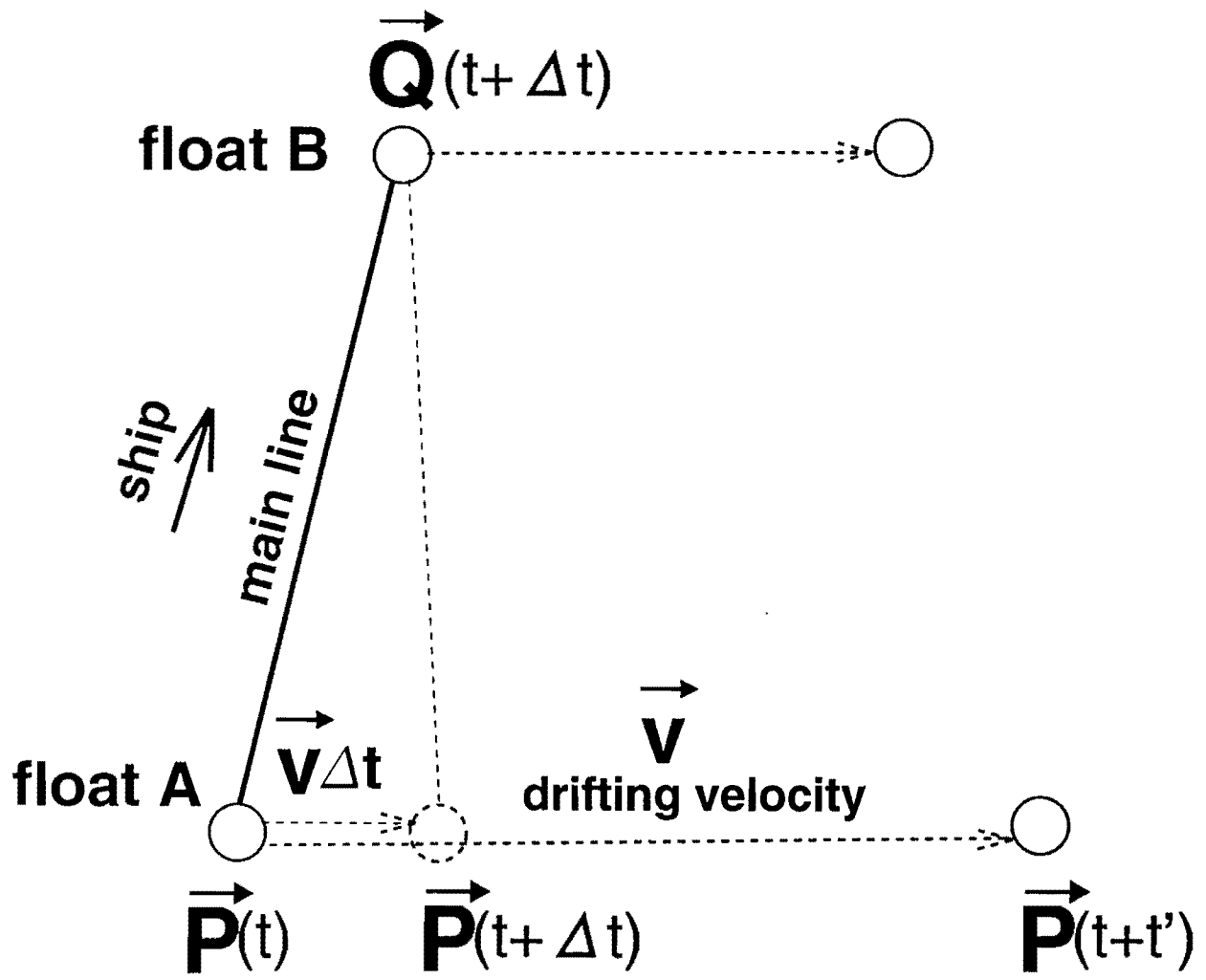


FIGURE 7. Estimation of the distance between a pair of floats. Float A is launched at time t , and retrieved at $t + t'$. The average drifting speed (V) is $(P(t + t') - P(t))/t'$. When float B is launched at time $t + \Delta t$ at position $Q(t + \Delta t)$, the position of float A ($P(t + \Delta t)$) is estimated to be at $P + V\Delta t$. The distance between floats A and B at time $t + \Delta t$ is estimated by the length of the vector $P(t + \Delta t)Q(t + \Delta t)$.

EXPERIMENT 1

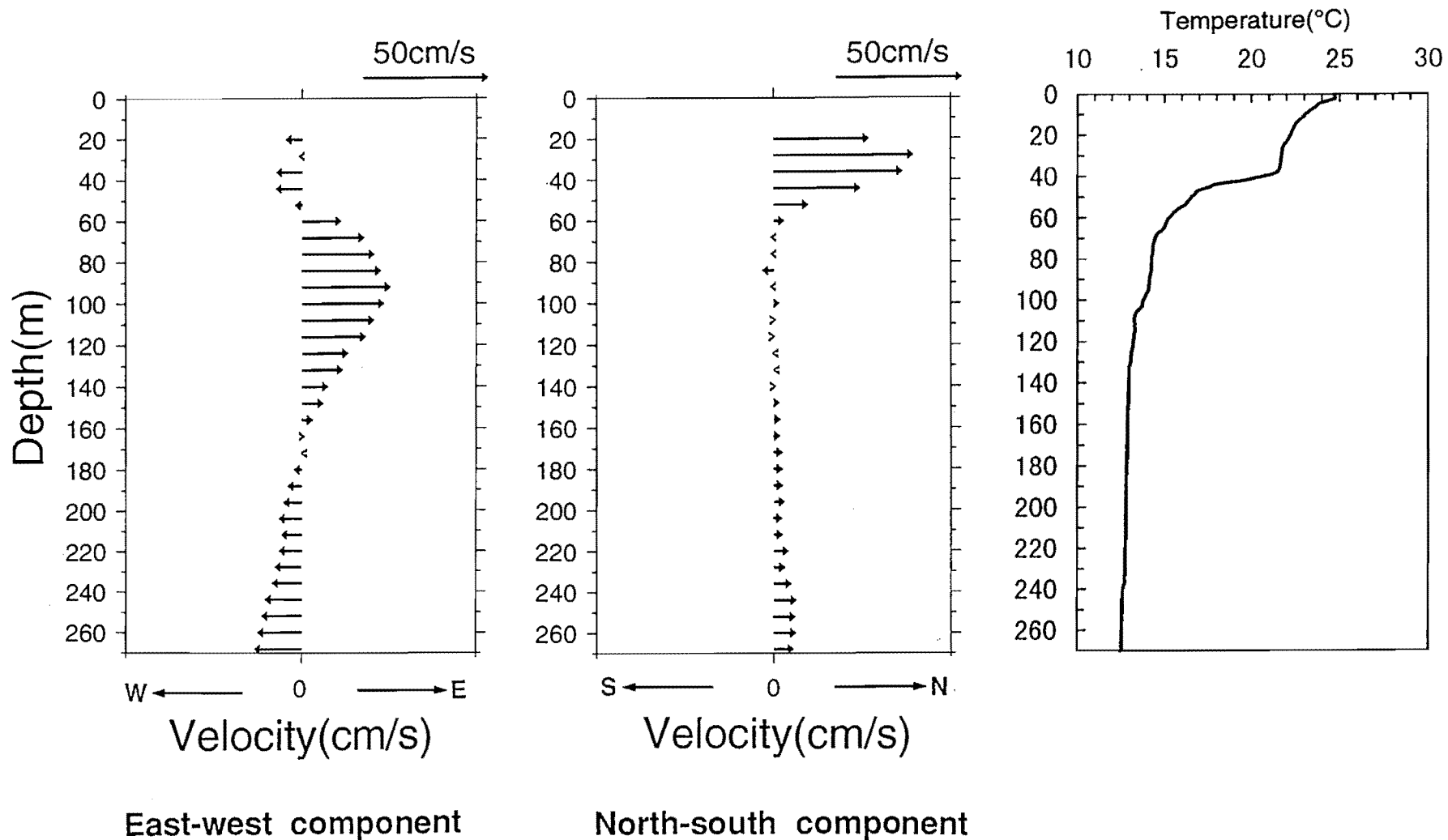
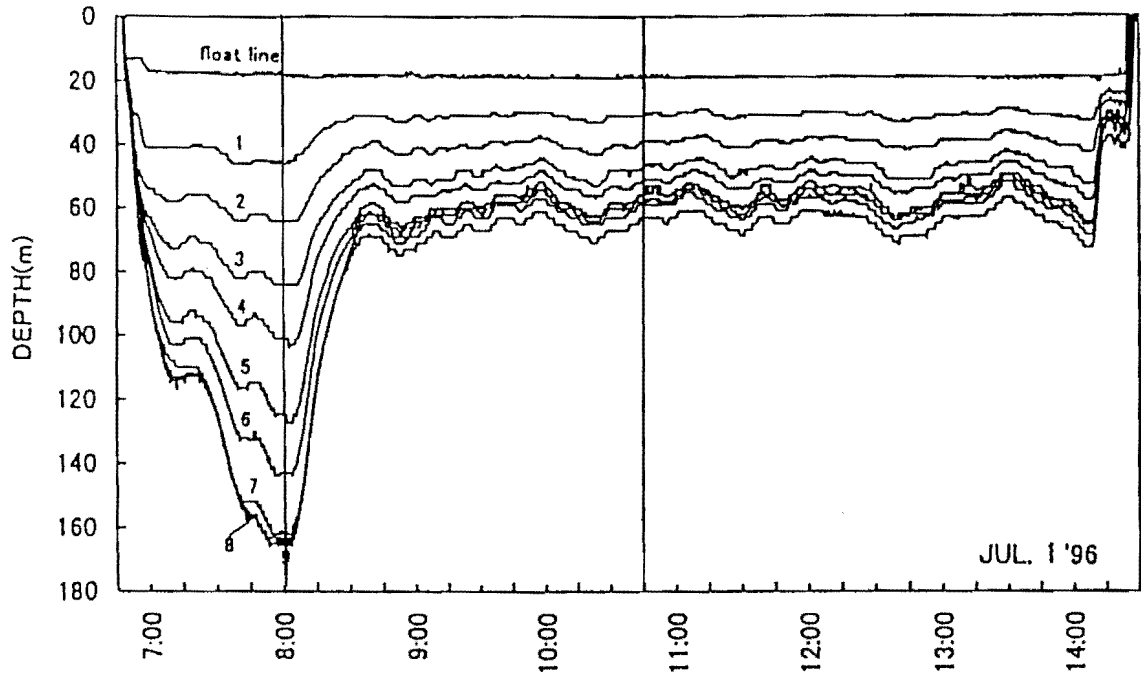


FIGURE 8. Vertical current and temperature profiles in Experiment 1.

Left/middle panels: Vertical profiles of zonal/meridional components of current measured by ADCP during the setting of the longline for Experiment 1 at intervals of 8 m, beginning at depth of 20 m.

Right panel: Vertical temperature profile obtained by XBT.

EXPERIMENT 1
branch #1 ~ #9



EXPERIMENT 1
branch #9 ~ #13

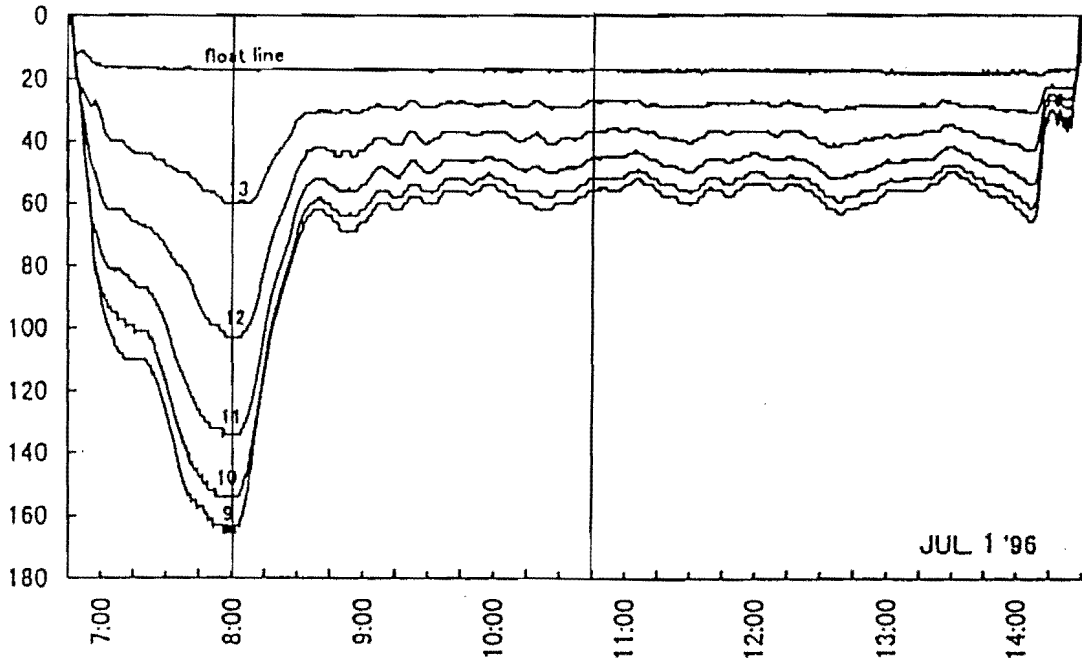


FIGURE 9. Time/depth records of micro-BTs in Experiment 1. Depth of branch lines at 10-second sampling intervals for lines 1-9 (upper panel) and 9-13 (lower panel).

EXPERIMENT 1

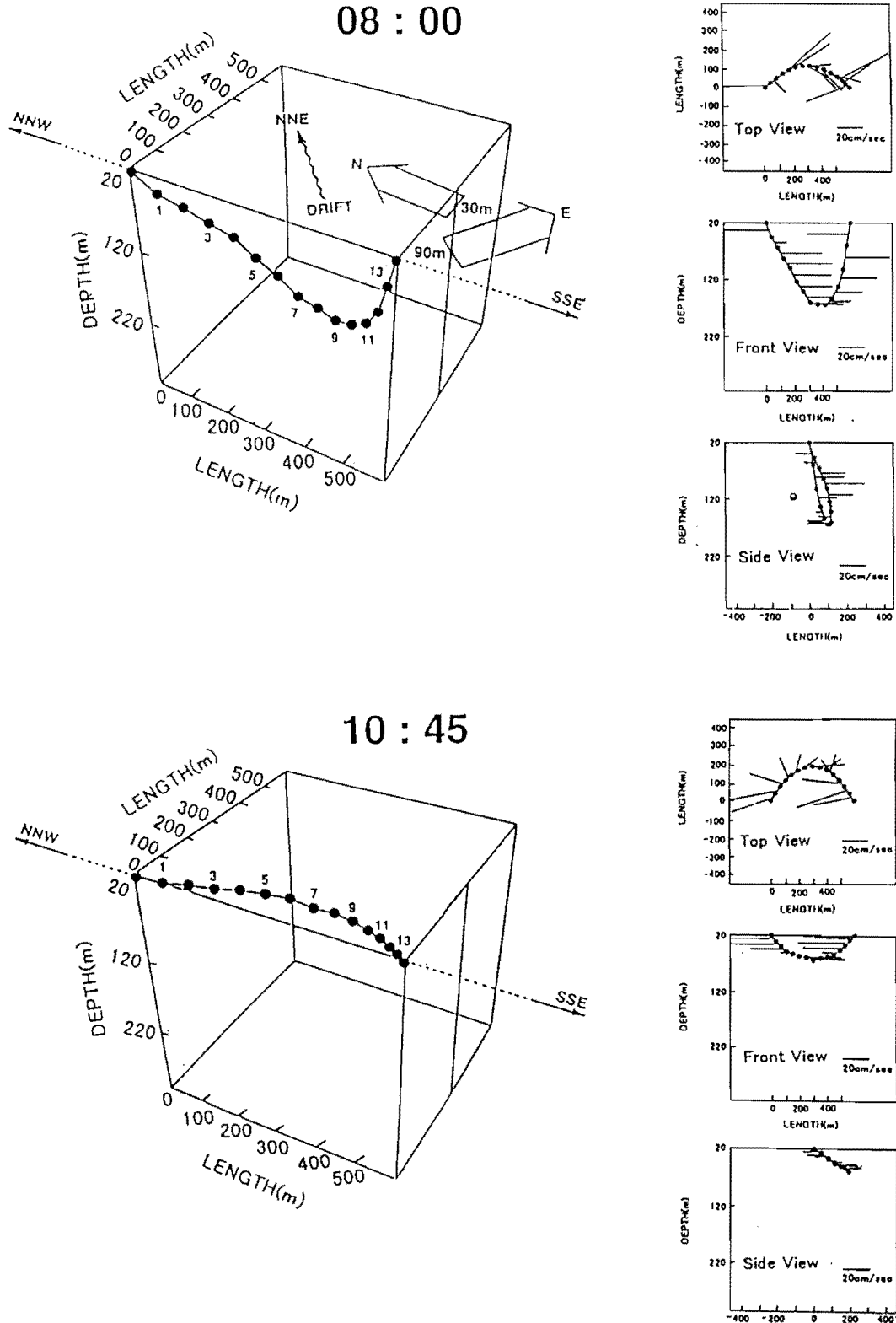


FIGURE 10. Calculated three-dimensional main line shapes for Experiment 1 at 08:00 (upper panel) and 10:45 (lower panel). In each panel, depths shallower than float line (*i.e.* 20 m) are not displayed. Vertical scale is half the horizontal scale. Solid circles denote the positions where micro-BTs are attached to the numbered branch lines. The direction of main line deployment and drift, and the upper and lower layer currents, are shown schematically (upper panel). Three planar views (top, front, and side) of the line are shown with relative current vectors at each segment of the line adjacent to the perspective views.

EXPERIMENT 2

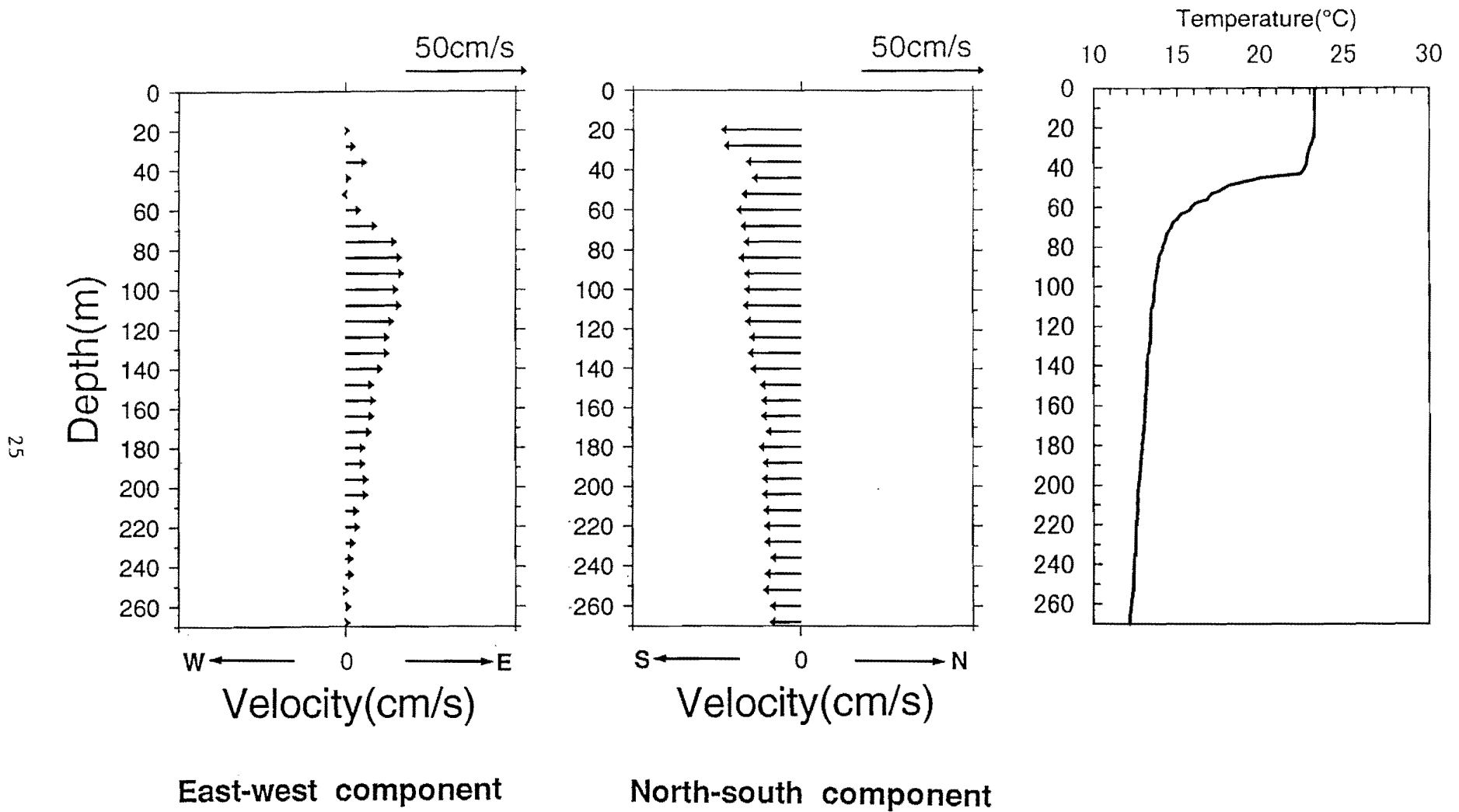


FIGURE 11. Vertical current and temperature profiles in Experiment 2.

Left/middle panels: Vertical profiles of zonal/meridional components of current measured by ADCP during the setting of the longline for Experiment 2 at intervals of 8 m, beginning at depth of 20 m.

Right panel: Vertical temperature profile obtained by XBT.

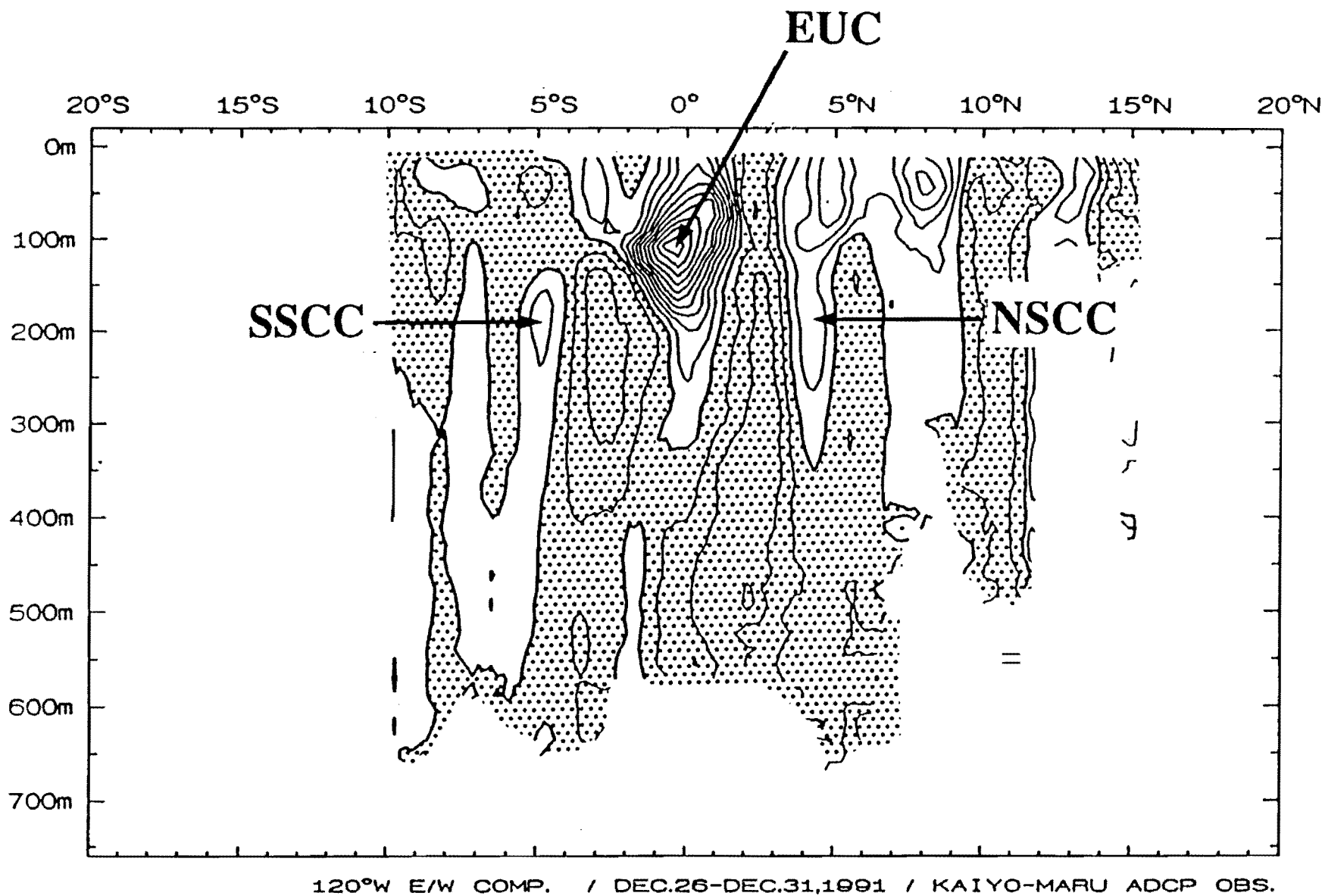
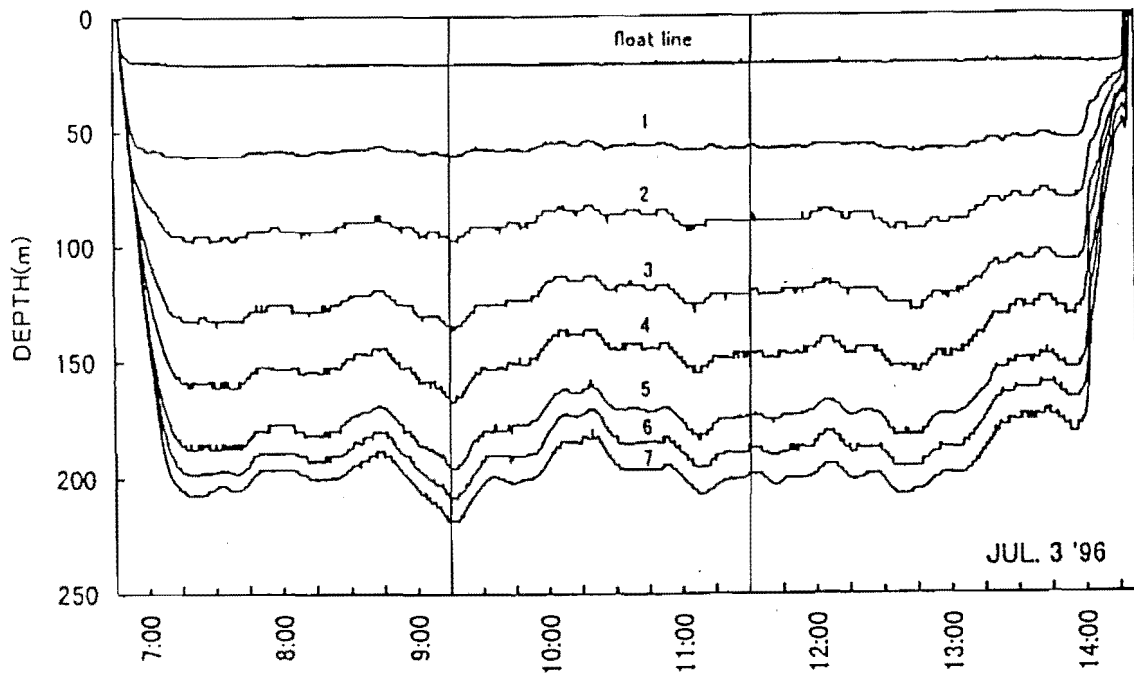


FIGURE 12. Zonal component of the current along 120°W obtained by ADCP. Contour interval is 10 cm/s and shaded portion indicates westward velocity. Eastward currents for SSCC (southern subsurface countercurrent), EUC (Equatorial Undercurrent), and NSCC (Northern Subsurface Countercurrent) are labeled (from Watanabe and Mizuno 1993).

EXPERIMENT 2
branch #1 ~ #7



EXPERIMENT 2
branch #7 ~ #13

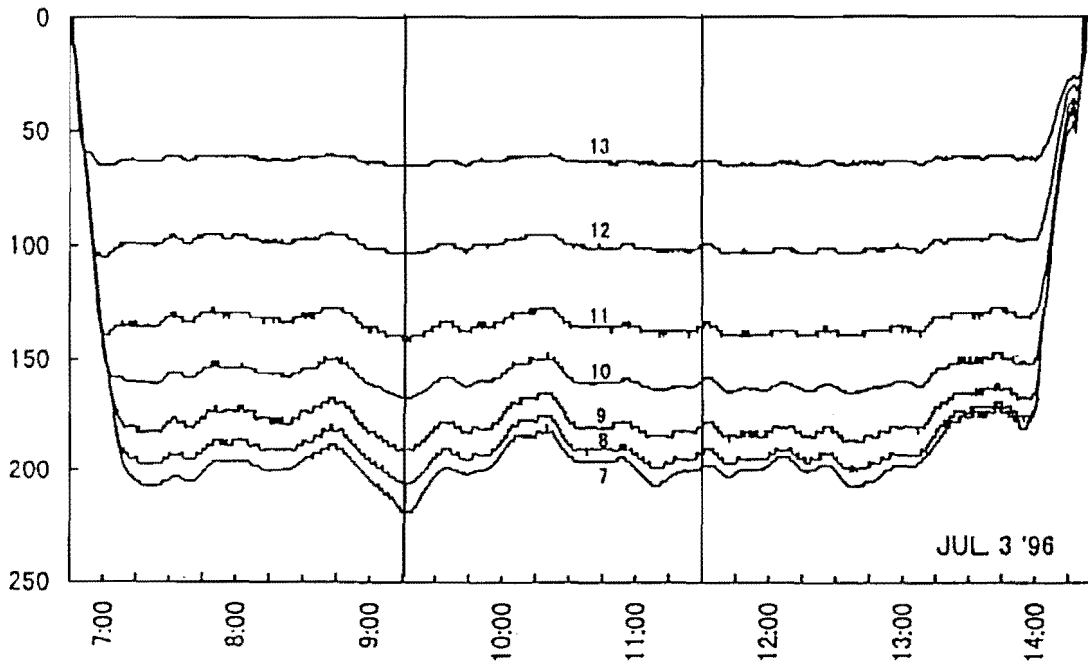
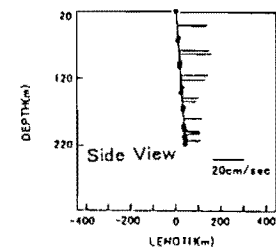
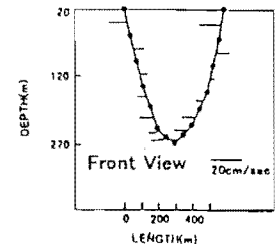
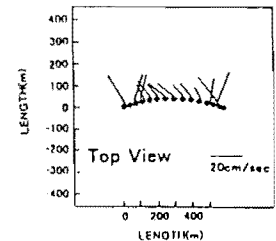
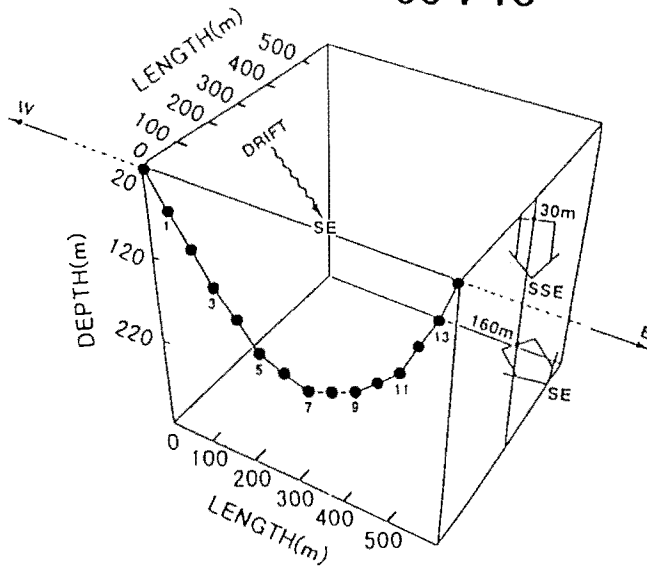


FIGURE 13. Time/depth records of micro-BTs in Experiment 2. Depth of branch lines at 10-second sampling intervals for lines 1-9 (upper panel) and 9-13 (lower panel).

EXPERIMENT 2

09 : 15



11 : 30

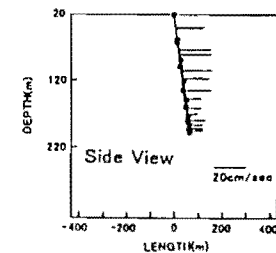
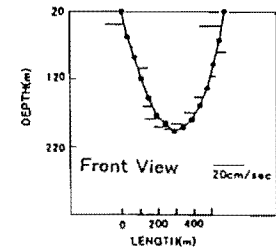
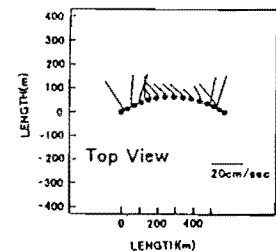
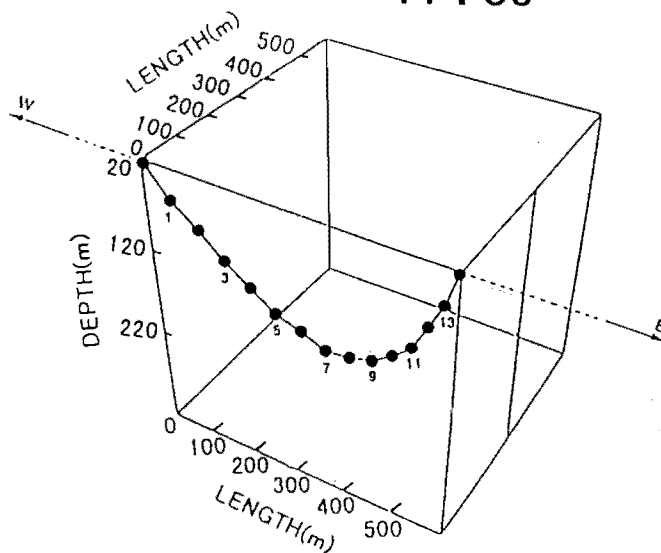


FIGURE 14. Calculated three dimensional main line shapes for Experiment 2 at 9:15 (upper panel) and 11:30 (lower panel). In each panel, depths shallower than float line (*i.e.* 20 m) are not displayed. Vertical scale is half the horizontal scale. Solid circles denote the positions where micro-BTs are attached to the numbered branch lines. The direction of main line deployment and drift, and the upper and lower layer currents, are shown schematically (upper panel). Three planar views (top, front, and side) of the line are shown with relative current vectors at each segment of the line adjacent to the perspective views.

EXPERIMENT 3

29

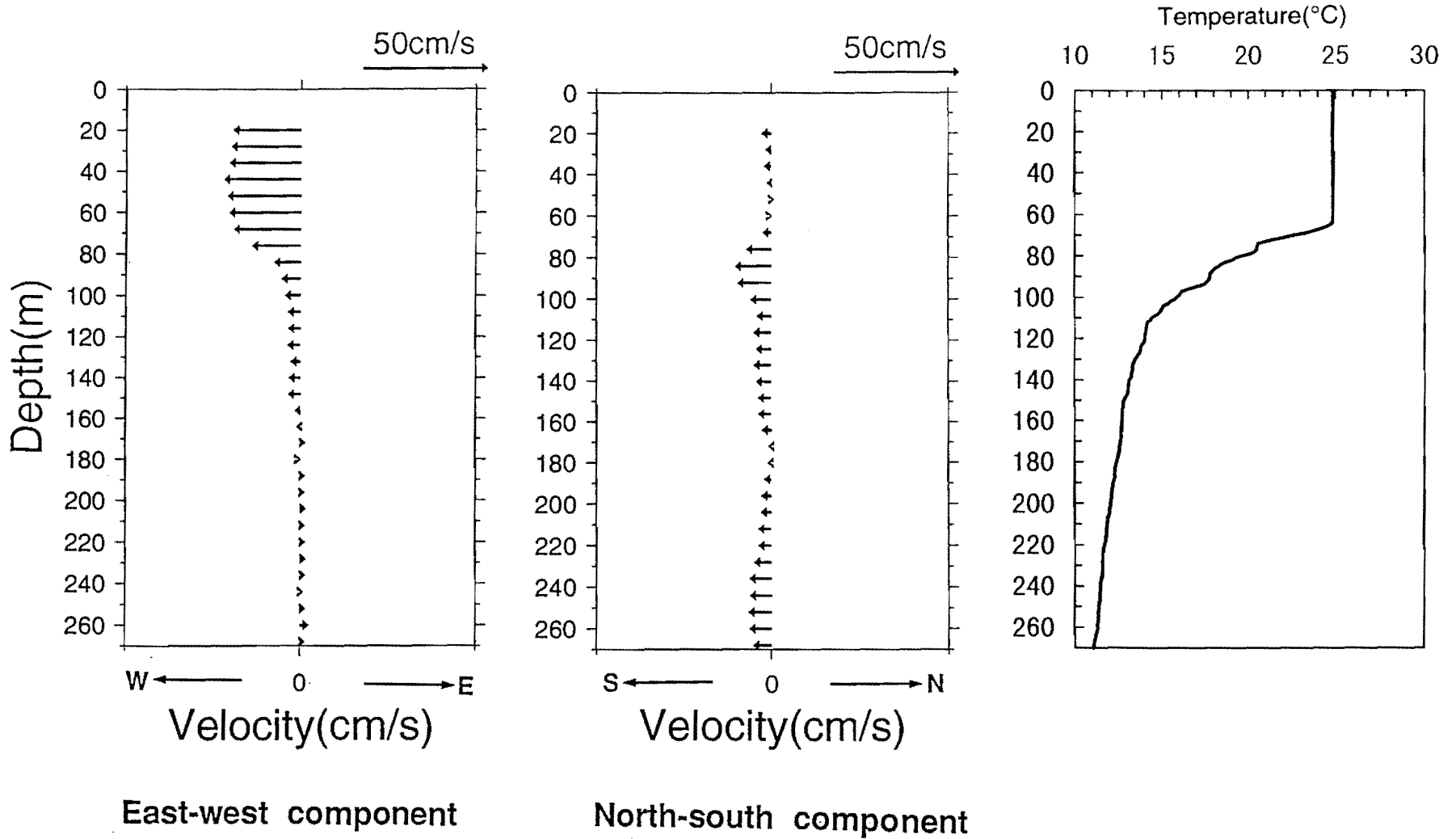
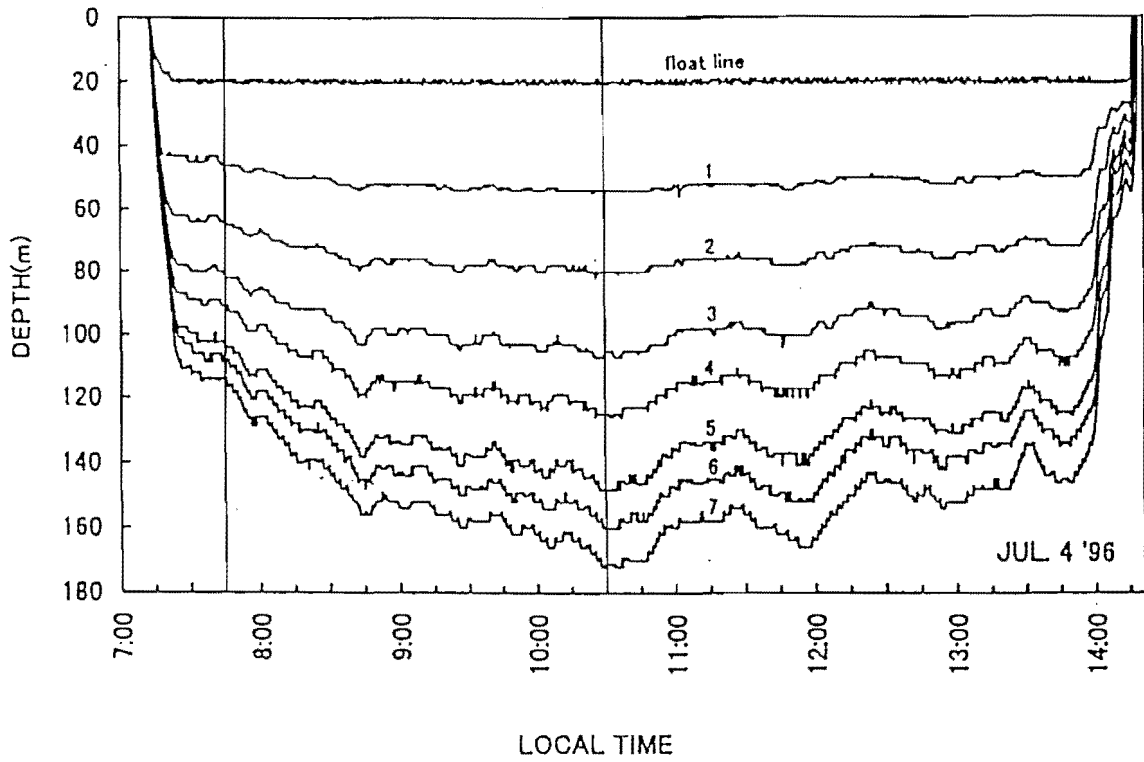


FIGURE 15. Vertical current and temperature profiles in Experiment 3. Left/middle panels: Vertical profiles of zonal/meridional components of current measured by ADCP during the setting of the longline for Experiment 1 at intervals of 8 m, beginning at depth of 20 m. Right panel: Vertical temperature profile obtained by XBT.

EXPERIMENT 3
branch #1 ~ #7



EXPERIMENT 3
branch #7 ~ #13

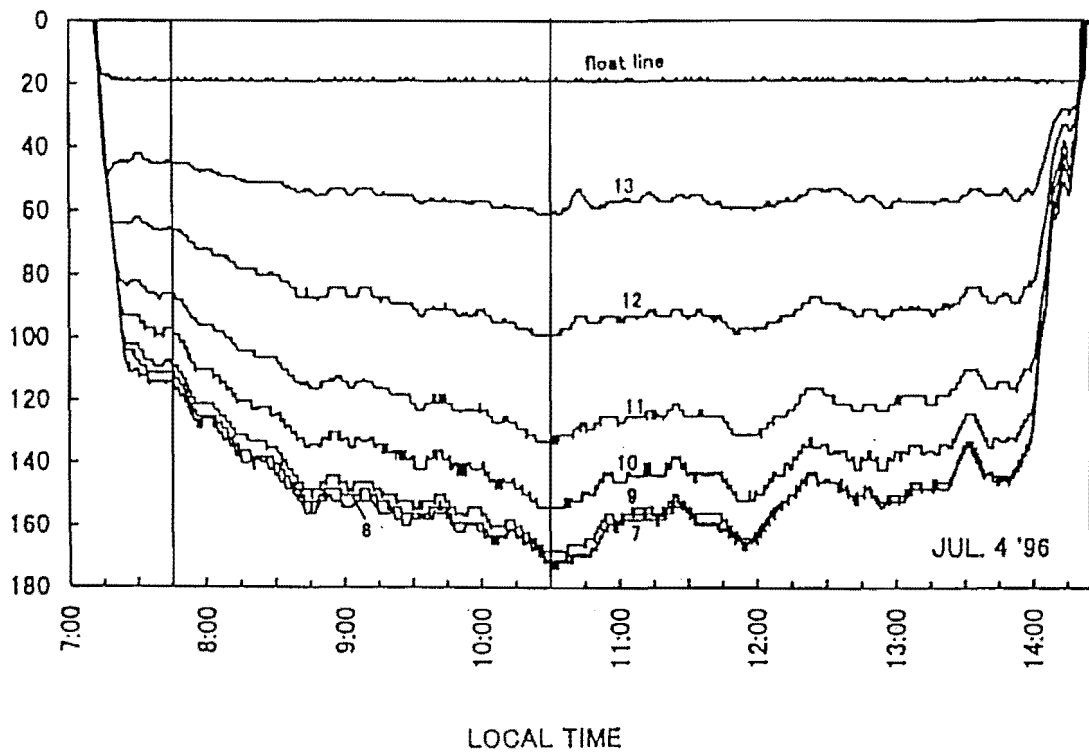
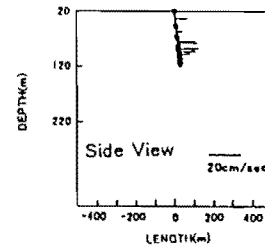
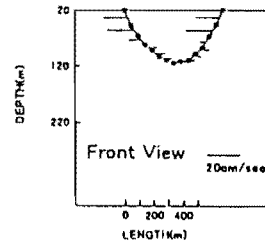
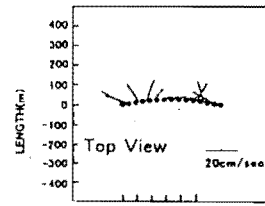
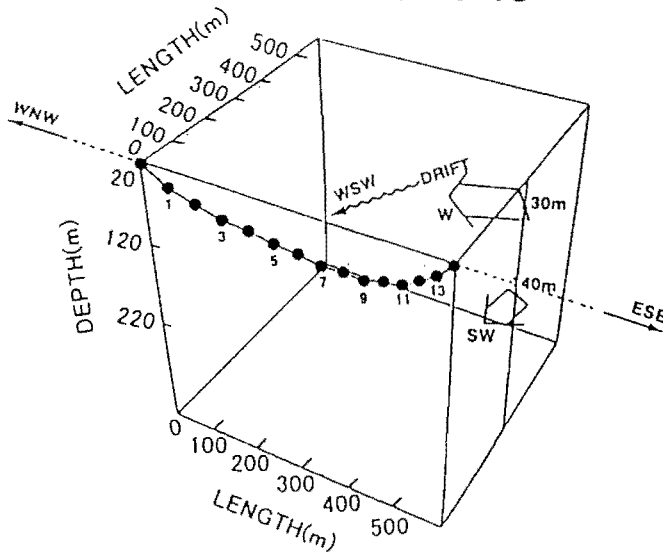


FIGURE 16. Time/depth records of micro-BTs in Experiment 3. Depth of branch lines at 10-second sampling intervals for lines 1-9 (upper panel) and 9-13 (lower panel).

EXPERIMENT 3

07 : 45



10 : 30

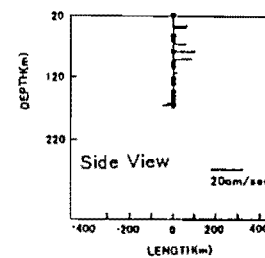
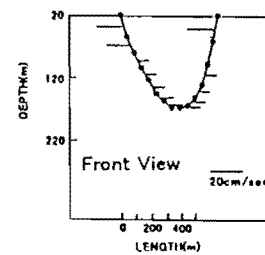
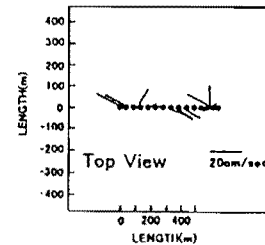
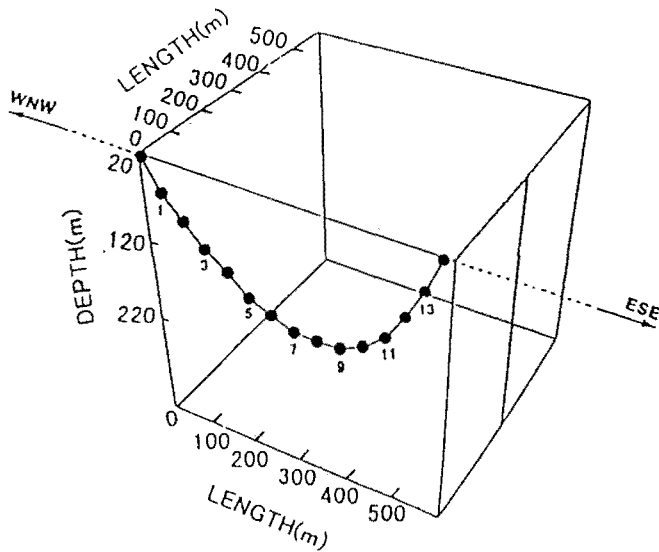


FIGURE 17. Calculated three dimensional main line shapes in Experiment 3 at 07:45 (upper panel) and 10:30 (lower panel). In each panel, depths shallower than float line (*i.e.* 20 m) are not displayed. Vertical scale is half the horizontal scale. Solid circles denote the positions where micro-BTs are attached to the numbered branch lines. The direction of main line deployment and drift, and the upper and lower layer currents, are shown schematically (upper panel). Three planar views (top, front, and side) of the line are shown with relative current vectors at each segment of the line adjacent to the perspective views.

TABLE 1. Outline of experiments.

Experiment 1	
Date/Time(Local time)	1996/07/01 04:40 - 19:25
Location(Start/End)	0°30.5'N, 100°10.0'W, - 0°42.0'N, 100°05.1'W
Longline Spec.	54 baskets, 13 branch lines / basket
Experimental basket	#5
Sea-surface wind	Calm
Wave height	0m
Experiment 2	
Date/Time(Local time)	1996/07/03 04:33 - 18:23
Location(Start/End)	5°21.2'S, 102°06.7'W, - 5°23.2'S, 102°02.9'W
Longline Spec.	54 baskets, 13 branch lines / basket
Experimental basket	#5
Sea-surface wind	ESE/3
Wave height	1m
Experiment 3	
Date/Time(Local time)	1996/07/04 04:32 - 19:27
Location(Start/End)	6°29.9'S, 103°22.3'W, - 6°30.3'S 103°27.5'W
Longline Spec.	54 baskets, 13 branch lines / basket
Experimental basket	#5
Sea-surface wind	E/5
Wave height	2m

TABLE 2. Specification of basket of longline.

	dimension	density/weight	material
Main line	53m × 0.42cm (in diameter)*		1.4
SuperMansen			
Float line	25m × 0.42cm (in diameter)	1.4	SuperMansen
Branch line	20m × 0.45cm (in diameter)	1.6	Tetron
Lashing	10m × 0.20cm (in diameter)	6.8	iron
Wire	2m × 0.10cm (in diameter)	6.8	iron
Float	30cm (in diameter)	30kg**	plastic
Hook	-	20g	iron
Snap	-	40g	iron

* a basket

** buoyancy

TABLE 3. Shortening rates.

Experiment #	Launching	Retrieving	*
1	0.79	0.82	(0.85)
2	0.86	0.82	(0.83)
3	10.1	0.86	(0.95)

* Values in parenthesis are estimated by the ratio of averaged releasing speed of main line and ship speed.

APPENDIX A

A METHOD TO FIND THE SMOOTHEST SHAPE FOR THE LINE

The shape of the main line can be expressed by a chain of N unit vectors (see text, Equation (3)):

$$\vec{V}_i = (r_i \cos \theta_i, r_i \sin \theta_i, d_i) \quad (i = 1, 2, \dots, N) \quad (\text{A1})$$

The coordinates of the endpoints of a unit vector are P_0 , which is located at the origin, and P_N , which is located at $(KN, 0, 0)$. The distance between the endpoints can be expressed as:

$$\overrightarrow{P_0 P_N} = \sum_{i=1}^N \vec{V}_i = \left(\sum_{i=1}^N r_i \cos \theta_i, \sum_{i=1}^N r_i \sin \theta_i, \sum_{i=1}^N d_i \right) = (KN, 0, 0) \quad (\text{A2})$$

where

$$\sum_{i=1}^N r_i \cos \theta_i = KN, \quad (\text{A3})$$

$$\sum_{i=1}^N r_i \sin \theta_i = 0, \quad (\text{A4})$$

and

$$\sum_{i=1}^N d_i = 0$$

The smoothest shape is defined as that which minimizes the sum of squared curvature at each point. Note that by definition the curvature is zero on an arm of the folding rule, and it can not be defined mathematically at the junction points, or junctions, of the arms because the derivatives are not continuous at the points. Thus, we approximated the curvature at junction points as:

$$|\vec{V}_i - \vec{V}_{i-1}| \quad (\text{A5})$$

Let T be the sum of the squared approximations of curvature at each point, then:

$$T = \sum_{i=2}^N (\vec{V}_i - \vec{V}_{i-1})^2 = 2(N-1) - 2 \sum_{i=2}^N \vec{V}_i \cdot \vec{V}_{i-1} \quad (\text{A6})$$

Substituting (A1) into the above equation and rearranging,

$$T = 2(N-1) - 2 \sum_{i=2}^N r_{i-1} r_i \cos(\theta_{i-1} - \theta_i) \quad (\text{A7})$$

To minimize T given (A3) and (A4), we solve for the a set of θ_i ($i = 1, 2, \dots, N$) that maximizes:

$$\sum_{i=2}^N r_{i-1} r_i \cos(\theta_{i-1} - \theta_i) \quad (\text{A8})$$

This is a standard problem in non-linear optimization. Since it is generally difficult to obtain the solutions by analytical methods, they are usually obtained using numerical methods. We used the multiplier method of Ohno and Isoda (1990).

Since a set of solutions θ_i is not unique, in that equation (A8) is mathematically equivalent for a pair of solutions that are symmetric about the X - Z plane. The correct solution is chosen from the pair by accounting for hydrographic conditions.

APPENDIX B

CRITERIA FOR SELECTING THE NUMBER OF SEGMENTS FOR THE MODEL

Considering the location of the m th junction point as a point vector $\overrightarrow{OP_m}$, it can be written as:

$$\overrightarrow{OP_m} = \left(\sum_{i=1}^m r_i \cos \theta_i, \sum_{i=1}^m r_i \sin \theta_i, \sum_{i=1}^m d_i \right) \quad (B1)$$

where d_i and r_i are as previously given.

Suppose that a point Q is on a catenary curve and that its distance from the origin O along the curve is s . Then the vector \overrightarrow{OQ} may be written as

$$\overrightarrow{OQ} = (f(s), 0, g(s)), \quad (B2)$$

and

$$f(s) = \frac{1}{a} \log(as - b + \sqrt{(as - b)^2 + 1}) + c,$$

$$g(s) = \frac{1}{a} \cosh(f(s))$$

where a , b , and c are the constants derived from total length N and the shortening rate K . Then for corresponding points P_m and Q on the folding-rule model and the catenary, P_mQ is the distance between the points. The sum of these squared distances provides a measure of the overall difference between the shapes. Although it would be possible to calculate the sum of the squared distances for all pairs of corresponding points along the catenary and the model, we calculated only the sum for the junction points in order to minimize the calculations. The sum of squares is as follows:

$$\frac{1}{N} \sum_{m=1}^N P_mQ^2 = \sum_{m=1}^N \left\{ \left(f(m) - \sum_{i=1}^m r_i \cos \theta_i \right)^2 + \left(\sum_{i=1}^m r_i \sin \theta_i \right)^2 \right\} \quad (B3)$$

A set of θ_i which minimizes the right side of this equation under the constraints in equations A3 and A4 can be obtained with non-linear optimization techniques, as previously discussed. The folding-rule model will be symmetrical, because the catenary to be fitted is symmetrical. This means that the symmetrical relationship ($\theta_i = \theta_{n-i}$) is within a solution set θ_i , and the number of variables to be estimated is actually halved.

Suppose the sum of squared distances above equals E . Then, since both the catenary curve and the folding-rule model have the same total length, E should be divided by the total length to normalize the error. Thus, the normalized error for fitting of the model is given by:

$$\epsilon_N = \frac{E}{N} \quad (B4)$$

